MAT_213 User Guide

(Version 1.3.6)

A User Guide for *MAT_COMPOSITE_TABULATED_PLASTICITY_DAMAGE in LS-DYNA®

S.D. Rajan, C. Hoffarth, B. Khaled, L. Shyamsunder, and A. Maurya
Computational and Experimental Mechanics Laboratory
School of Sustainable Engineering & the Built Environment
Arizona State University
Tempe, AZ 85287

Last Update: June 2023

Table of Contents

List of Figures

List of Tables

List of Abbreviations

Abbreviation	Remarks
C1, C2, C3	Compression tests in 1-direction, 2-direction, 3-direction
FRC	Flow Rule Coefficients
GTFC	Generalized Tabulated Failure Criterion
NRMSE	Normalized Root Mean Square Error
O12, O23, O13	Off-axis tests in the 12, 23, 13 planes
PFC	Puck Failure Criterion
PMD	Principal Material Directions referred to as 1, 2, 3 for orthotropic composites
PMP	Principal Material Planes referred to as 12, 23, 13 planes (see PMD)
QS-RT	Quasi-Static Room Temperature
S12, S23, S13	Shear tests in the 12, 23, 13 planes
T1, T2, T3	Tension tests in 1-direction, 2-direction, 3-direction
TWFC	Tsai-Wu Failure Criterion
VEVP	Visco-Elastic Visco-Plastic behavior

Nomenclature

Symbol	Remarks
σ	Cauchy stress (true stress)
σ^{eff}	Effective stress
ε	Strain
E	Young's modulus
G	Shear's modulus
ν	Poisson's Ratio
f	Yield surface function
a, F	Yield function coefficients
h	Plastic potential function (flow rule)
H	Flow rule coefficient
d_{kl}^{ij}	Damage parameter where ij is the direction in which the damage is induced and kl is the loading direction
β_t	Taylor-Quinney coefficient
c_p	Specific heat
Superscripts	
p	Plastic component
e	Elastic component
C	Compression
T	Tension
Subscripts	
1, 2, 3	Principal material directions (same as DYNA's a, b, c)

1. Introduction

Modeling and simulation of composite structures during an impact event is a huge challenge given the wide variety of composites and the associated complexity in characterization of the behavior of the constituent materials as well as the interaction between them. While composites have been in use for decades in a variety of industries such as civil structures, automotive and aerospace, building a predictive model is still daunting. Some of the challenges facing the industry are diverse and need to be addressed [Kaddour et al., 2014]. They include (a) shorter life cycles, (b) automated manufacture, (c) production of high volumes, (d) integrating 3D structures into 3D architectures, (e) development of alternative materials, and (f) meeting climate change targets. In the United States, several governmental agencies (including NASA and the FAA) have recognized the importance of building a framework for a composites system by forming a public–private consortium. A press release [NASA, 2016] states that "NASA formed the consortium in support of the Advanced Composites Project, which is part of the Advanced Air Vehicles Program in the agency's Aeronautics Research Mission Directorate. The project's goal is to reduce product development and certification timelines by 30 percent for composites infused into aeronautics applications." A major reason for these challenges is the lack of mature material models that should be able to predict, with some degree of certainty, the deformation, damage and failure of composite systems.

The initial development of MAT_213 started with funding from the FAA in 2012. Subsequently, additional funding was obtained from NASA as a part of the Advanced Composites Project (ACP) in 2015. The work was undertaken with a view to developing theory, algorithms, experimental techniques and computer implementation in a commercial program to reduce the total time taken for the development and certification of new composites and structures. Currently, the certification process can take between 10-20 years, with a goal of this research program to reduce certification time to 3-5 years, with funding from the FAA and NASA.

The user guide is divided into several parts. First, very briefly, the components of the constitutive model – deformation, damage and failure, are explained in Chapter 2. Chapter 3 is devoted to using MAT_213 with reference to the input data for the deformation, damage and failure sub-models. Chapter 4 discusses some of the major error and warning messages associated with MAT_213. Key references are listed at the end of the document.

2. Theoretical Background

MAT_213 constitutive model is divided into a deformation sub-model, a damage sub-model and a failure sub-model (Fig. 2.1). Such a partitioning allows for the elastic and plastic deformations to be captured by the deformation model and the reduction in stiffness to be captured by the damage model, with the failure model being used to erode elements from the finite element (FE) model. In other words, the deformation sub-model simulates the nonlinear material response of the composite (due to either deformation or damage mechanisms), the damage sub-model simulates the nonlinear unloading/reloading due to stiffness reduction, and the failure sub-model predicts when the failure criteria is satisfied at a stress/strain Gauss point and erodes the element appropriately. The response of a system can then be monitored as the finite element calculations are processed through the deformation and damage models so that the failure model can be used to carry out failure predictions. The deformation model generalizes the Tsai–Wu failure criteria and extends it into a strain-hardening-based orthotropic yield function with a non-associated flow rule. A strain equivalent formulation is utilized in the damage model that permits the plasticity and damage calculations to be uncoupled and captures the nonlinear unloading and local softening of the stress–strain response. A diagonal damage tensor is defined to account for the directionally dependent variation of damage. However, in composites, it has been found that loading in one direction can lead to damage in multiple coordinate directions. To account for this phenomenon, the terms in the damage matrix are semi-coupled, as explained later, such that the damage in a particular coordinate direction is a function of the stresses and plastic strains in all of the coordinate directions. The overall framework is driven by experimentally obtained tabulated temperature- and rate-dependent stress–strain data as well as data that characterizes the damage matrix and failure.

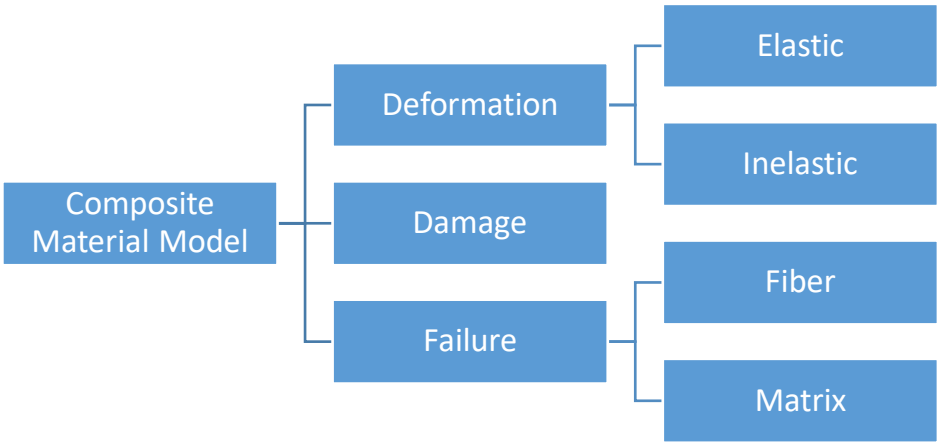

Fig. 2.1. MAT_213 architecture

The current version of MAT_213 supports two finite elements – solid elements and thin shell elements. Differences in the input and implementation of the two element types are discussed where appropriate.

2.1 Deformation Sub-Model

A quadratic yield function which has the form of the commonly used Tsai-Wu composite failure model is defined as

$$f(\sigma) = a + \begin{pmatrix} F_1 & F_2 & F_3 & 0 & 0 & 0 \end{pmatrix} \begin{bmatrix} \sigma_{11} \\ \sigma_{22} \\ \sigma_{33} \\ \sigma_{12} \\ \sigma_{23} \\ \sigma_{31} \end{bmatrix} + \begin{bmatrix} \sigma_{11} \\ \sigma_{22} \\ \sigma_{33} \\ \sigma_{12} \\ \sigma_{23} \\ \sigma_{31} \end{bmatrix}^T \begin{bmatrix} F_{11} & F_{12} & F_{13} & 0 & 0 & 0 \\ F_{12} & F_{22} & F_{23} & 0 & 0 & 0 \\ F_{13} & F_{23} & F_{33} & 0 & 0 & 0 \\ 0 & 0 & 0 & F_{44} & 0 & 0 \\ 0 & 0 & 0 & 0 & F_{55} & 0 \\ 0 & 0 & 0 & 0 & 0 & F_{66} \end{bmatrix} \begin{bmatrix} \sigma_{11} \\ \sigma_{22} \\ \sigma_{33} \\ \sigma_{12} \\ \sigma_{23} \\ \sigma_{31} \end{bmatrix} \tag{2.1}$$

where $a = -1$. The yield function coefficients, F_{ij}, depend on the current yield stress values and are calculated as

$$\begin{aligned} F_1 &= \frac{1}{\sigma_{11}^T} - \frac{1}{\sigma_{11}^C} & F_{11} &= \frac{1}{\sigma_{11}^T \sigma_{11}^C} & F_{44} &= \frac{1}{\sigma_{12}^2} \\ F_2 &= \frac{1}{\sigma_{22}^T} - \frac{1}{\sigma_{22}^C} & F_{22} &= \frac{1}{\sigma_{22}^T \sigma_{22}^C} & F_{55} &= \frac{1}{\sigma_{23}^2} \\ F_3 &= \frac{1}{\sigma_{33}^T} - \frac{1}{\sigma_{33}^C} & F_{33} &= \frac{1}{\sigma_{33}^T \sigma_{33}^C} & F_{66} &= \frac{1}{\sigma_{31}^2} \end{aligned} \tag{2.2}$$

$$F_{12} = \frac{2}{\left(\sigma_{12}^{45}\right)^2} - \frac{F_1 + F_2}{\sigma_{12}^{45}} - \frac{1}{2}\left(F_{11} + F_{22} + F_{44}\right) \tag{2.3}$$

$$F_{23} = \frac{2}{\left(\sigma_{23}^{45}\right)^2} - \frac{F_2 + F_3}{\sigma_{23}^{45}} - \frac{1}{2}\left(F_{22} + F_{33} + F_{55}\right) \tag{2.4}$$

$$F_{13} = \frac{2}{\left(\sigma_{31}^{45}\right)^2} - \frac{F_1 + F_3}{\sigma_{31}^{45}} - \frac{1}{2}\left(F_{11} + F_{33} + F_{66}\right) \tag{2.5}$$

where the superscripts T, C and 45 denote data obtained from tension, compression and 45-degree off-axis tests, respectively.

A non-associated flow rule is used to compute the evolution of the components of plastic strain and the plastic potential function is defined as

$$h = \sqrt{H_{11}\sigma_{11}^2 + H_{22}\sigma_{22}^2 + H_{33}\sigma_{33}^2 + 2H_{12}\sigma_{11}\sigma_{22} + 2H_{23}\sigma_{22}\sigma_{33} + 2H_{31}\sigma_{33}\sigma_{11} + H_{44}\sigma_{12}^2 + H_{55}\sigma_{23}^2 + H_{66}\sigma_{31}^2} \tag{2.6}$$

where the H_{ij} terms are a set of constant coefficients with the coefficients defined as input parameters in the model.

The reader is urged to refer to the following documents to gain an understanding not only of the theoretical details of the deformation sub-model but also how to link the theory to generating the input file for LS-DYNA.

Start Here: (1) C. Hoffarth, PhD Dissertation, A Generalized Orthotropic Elasto-Plastic Material Model for Impact Analysis, Arizona State University, December 2016. This document is available here: https://www.tc.faa.gov/its/worldpac/techrpt/tctt17-54.pdf

(2) B. Khaled, PhD Dissertation, Experimental Characterization and Finite Element Modeling of Composites to Support a Generalized Orthotropic Elasto-Plastic Damage Material Model for Impact Analysis, August 2019. This document is available here: https://www.tc.faa.gov/its/worldpac/techrpt/tctt22-39.pdf

(3) T. Achstetter, PhD Dissertation, Development of a Composite Material Shell-Element Model for Impact Applications, George Mason University, Fall 2019. This document is available here: https://www.tc.faa.gov/its/worldpac/techrpt/tc19-50-p3.pdf.

(4) L. Shyamsunder, PhD Dissertation, Failure Modeling in an Orthotropic Plastic Material Model Under Static and Impact Loading, Arizona State University, Fall 2020. This document is available here: https://www.tc.faa.gov/its/worldpac/techrpt/tctt22-38.pdf

Journal Papers: (1) Hoffarth et al., 2016, 2017. (2) Goldberg et al., 2015. (3) Harrington et al., 2017, (4) Khaled et al., 2017a., (5) Shyamsunder et. al., 2022a, 2022b.

FAA Technical Reports: (1) C. Hoffarth, B. Khaled, L. Shyamsunder, and S. Rajan, Development of a Tabulated Material Model for Composite Material Failure, MAT213. Part 1: Theory, Implementation, Verification & Validation. DOT/FAA/TC-19/50, P1, Jan 2020. This document is available here: https://rosap.ntl.bts.gov/view/dot/57813/dot_57813_DS1.pdf.

(2) B. Khaled, L. Shyamsunder, N. Schmidt, C. Hoffarth and S. Rajan, Development of a Tabulated Material Model for Composite Material Failure, MAT213. Part 2: Experimental Tests to Characterize the Behavior and Properties of T800-F3900 Toray Composite. DOT/FAA/TC-19/50, P2. This document is available here: https://www.tc.faa.gov/its/worldpac/techrpt/tc19-50-p2.pdf.

NASA TM: (1) https://ntrs.nasa.gov/archive/nasa/casi.ntrs.nasa.gov/20150000901.pdf (2) https://ntrs.nasa.gov/archive/nasa/casi.ntrs.nasa.gov/20140017766.pdf

2.2 Damage Sub-Model

The damage model is used to relate the true (damaged) stress space to the effective (undamaged) stress space. The true stress space is related directly to what is measured during the experiments. The effective stress space is related to the undamaged material. Essentially, the effective stress space is generated by assuming the inelastic deformations are due to both damage and plasticity. The true and effective stress spaces can be related by a damage tensor as

$$\begin{pmatrix} \sigma_{11} \\ \sigma_{22} \\ \sigma_{33} \\ \sigma_{12} \\ \sigma_{23} \\ \sigma_{13} \end{pmatrix} = \begin{bmatrix} M_{11} & M_{12} & M_{13} & M_{14} & M_{15} & M_{16} \\ M_{21} & M_{22} & M_{23} & M_{24} & M_{25} & M_{26} \\ M_{31} & M_{32} & M_{33} & M_{34} & M_{35} & M_{36} \\ M_{41} & M_{42} & M_{43} & M_{44} & M_{45} & M_{46} \\ M_{51} & M_{52} & M_{53} & M_{54} & M_{55} & M_{56} \\ M_{61} & M_{62} & M_{63} & M_{64} & M_{65} & M_{66} \end{bmatrix} \begin{pmatrix} \sigma_{11}^{eff} \\ \sigma_{22}^{eff} \\ \sigma_{33}^{eff} \\ \sigma_{12}^{eff} \\ \sigma_{23}^{eff} \\ \sigma_{13}^{eff} \end{pmatrix} \tag{2.7}$$

where σ_{ij} is the true stress and σ_{ij}^{eff} is the effective stress. Eq. 2.7 shows a full damage tensor which could lead to multiaxial stress states in the effective space that correspond to uniaxial states in the true space. This finding or result is non-physical. Therefore, a semi-coupled, directionally dependent tensor is used in the current implementation as

$$\begin{pmatrix} \sigma_{11} \\ \sigma_{22} \\ \sigma_{33} \\ \sigma_{12} \\ \sigma_{23} \\ \sigma_{13} \end{pmatrix} = \begin{bmatrix} M_{11} & 0 & 0 & 0 & 0 & 0 \\ 0 & M_{22} & 0 & 0 & 0 & 0 \\ 0 & 0 & M_{33} & 0 & 0 & 0 \\ 0 & 0 & 0 & M_{44} & 0 & 0 \\ 0 & 0 & 0 & 0 & M_{55} & 0 \\ 0 & 0 & 0 & 0 & 0 & M_{66} \end{bmatrix} \begin{pmatrix} \sigma_{11}^{eff} \\ \sigma_{22}^{eff} \\ \sigma_{33}^{eff} \\ \sigma_{12}^{eff} \\ \sigma_{23}^{eff} \\ \sigma_{13}^{eff} \end{pmatrix} \tag{2.8}$$

Each of the terms in the damage tensor in Eq. 2.8 are dependent on all the plastic strains which are induced in the material, e.g. $M_{11} = M_{11}\left(\varepsilon_p^{11}, \varepsilon_p^{22}, \varepsilon_p^{33}, \varepsilon_p^{12}, \varepsilon_p^{23}, \varepsilon_p^{13}\right)$. The damage parameters are tracked as a function of plastic strain. The semi-coupled nature of the damage tensor ensures that a uniaxial effective stress state does not result in a multiaxial true stress state. For full generalization, both normal and shear damage are attributed to all normal and shear terms. Additionally, no assumption is made regarding the symmetry of the material, meaning damage induced due to compression or tension loading in a given PMD is treated independently.

The reader is urged to refer to the following documents to gain an understanding not only of the theoretical details of the damage sub-model but also how to link the theory to the deformation sub-model, and to generating the input file for LS-DYNA.

Start Here: B. Khaled, PhD Dissertation, Experimental Characterization and Finite Element Modeling of Composites to Support a Generalized Orthotropic Elasto-Plastic Damage Material Model for Impact Analysis, August 2019. This document is available here: https://www.tc.faa.gov/its/worldpac/techrpt/tctt22-39.pdf

Journal Papers: (1) Khaled et al., 2017b, 2019a. (2) Goldberg et al., 2018a.

NASA TM: (1) https://ntrs.nasa.gov/archive/nasa/casi.ntrs.nasa.gov/20150019390.pdf (2) https://ntrs.nasa.gov/archive/nasa/casi.ntrs.nasa.gov/20160002089.pdf

2.3 Failure Sub-Model

Several traditional failure theories are supported – Tsai-Wu, and Puck [Deuschle and Kroplin, 2012] as well as the Generalized Tabulated Failure Criterion [Goldberg et al., 2018b; Shyamsunder et al., 2020a]. The failure checks take place at every stress/strain Gauss point and if the failure criterion is met, the element is marked for erosion.

The reader is urged to refer to the following documents to gain an understanding not only of the theoretical details of the failure sub-model but also how to link the theory to the deformation and damage sub-models, and to generate the input file for LS-DYNA.

Start Here: L. Shyamsunder, PhD Dissertation, Failure Modeling in an Orthotropic Plastic Material Model for Impact and Crush Analysis, Arizona State University, 2020. This document is available here: https://www.tc.faa.gov/its/worldpac/techrpt/tctt22-38.pdf

Journal Papers: (1) Shyamsunder et al., 2019, 2020a, 2020b. (2) Goldberg et al., 2018b.

NASA TM: (1) https://ntrs.nasa.gov/archive/nasa/casi.ntrs.nasa.gov/20170004667.pdf

3. Description of MAT_213 Input Parameters

The MAT_213 input deck (V1.3.5 and V1.3.6) takes the following form:

```
*MAT_213
$# Card 1
$#     mid        ro         Ea         Eb         Ec        PRba        PRca        PRcb
       213 1.4521E-4   23.46E6   1.066E6   0.966E6   0.016800   0.027000      0.4390
$# Card 2
$#     Gab        Gbc        Gac                  AOPT        MACF        FILT        VEVP
  0.5795E6   0.326E6   0.3477E6                 2.000       0.000         0.1           2
$# Card 3
$#      xp         yp         zp         a1         a2         a3
     0.000      0.000      0.000      0.000    -1.0000      0.000
$# Card 4
$#      v1         v2         v3         d1         d2         d3       beta      TCSYM
     0.000      0.000      0.000   1.000000      0.000      0.000      0.000          0
$# Card 5
$#     H11        H22        H33        H12        H23        H13        H44        H55
   0.00000    1.00000    1.00000   0.000000   -0.77600   0.000000    4.23900    15.3100
$# Card 6
$#     H66        LT1        LT2        LT3        LT4        LT5        LT6        LT7
   5.37180       1001       1002       1003       1004       1005       1006       1007
$# Card 7
$#     LT8        LT9       LT10       LT11       LT12        YSC      DFLAG         DC
      1008       1009       1010       1011       1012        100          0          0
$# Card 8
$#   FCTYPE        FV0        FV1        FV2        FV3        FV4        FV5        FV6
           0
$# Card 9
$#     FV7        FV8        FV9       FV10       FV11       FV12       FV13       FV14

$# Card 10
$#  BETA11     BETA22     BETA33     BETA44     BETA55     BETA66     BETA12     BETA23
      0.01       0.01       0.01       0.01       0.01       0.01       0.01       0.01
$# Card 11
$#  BETA13         cp        TQC       TEMP      PMACC
      0.01
```

Parameters highlighted in green are used exclusively by LS-DYNA to perform internal computations (i.e. initial time step etc.). Parameters highlighted in blue are used in the MAT_213 plasticity algorithm. Parameters highlighted in orange are used in the MAT_213 damage algorithm. Parameters highlighted in red are used in the MAT_213 failure algorithm. All parameters are described in the LS-DYNA keyword manual.

MAT_213 is comprised of three sub-models: deformation, damage, and failure, each with their own set of input parameters. This section describes the techniques used to derive the input parameters for each sub-model as well as the expected format of the parameters. Data obtained for the T800/F3900 carbon fiber/epoxy resin unidirectional composite [Khaled et al., 2017a; Toray, 2020] is used to illustrate the techniques.

The following table shows the important differences between the solid and the thin shell element with respect to MAT_213 input and computations.

Table 3.1. Feature comparison between solid and shell implementations

Input/Feature	Solid Element	Shell Element
Testing to generate tabulated data	Minimum of 12 tests are required. See Table 3.2 for details.	Minimum of 5 tests are required – T1, T2, C1, C2, S12. See Table 3.2 for details. 1-2 plane Off-axis stress-strain curve is optional. If not provided, the yield function coefficient for the interaction is taken as zero.
Deformation Model – only linear behavior	Available	Not available
Deformation Model – linear + nonlinear behavior	Available via visco-elastic visco-plastic formulation	Available via visco-elastic visco-plastic formulation
Flow Rule Coefficients	All nine FRC required	Only H_{11}, H_{22}, H_{12}, H_{23}, H_{31} and H_{44} needed.
Damage Sub-model	Available	Available
Failure Sub-model	User can choose from (1) PFC (2) TWFC (3) GTFC	User can choose from (1) TWFC (2) GTFC

3.1 Deformation Sub-Model

The input needed to drive the plasticity-based deformation sub-model can be derived from a set of twelve experiments performed under uniaxial stress conditions: uniaxial tension in each of the three PMDs, uniaxial compression in each of the three PMD, pure shear in each of the three principal material planes (PMP), and 45° off-axis tension or compression in each of the three PMPs. The PMDs are referred to as the 1, 2, and 3 directions respectively (analogous to the a, b, and c material directions in the LS-DYNA keyword user's manual). For a general orthotropic material, twelve experiments are expected to be performed under quasi-static and room temperature (QS-RT) conditions using actual laboratory testing or virtual testing. In addition, each of the twelve experiments may be performed at various combinations of temperature and strain rate to provide additional data to MAT_213. Table 3.2 shows what curves are required and what are optional.

However, if one wants to use shell elements, the required number of experiments can be reduced to five. These five experiments are uniaxial tension in each of the two in-plane PMDs, uniaxial compression in each of the in-plane PMDs and in-plane pure shear. The requirement of in-plane off-axis testing is optional for shell elements. The deformation sub-model assumes that the

interactive coefficient in the yield function is zero if the in-plane off-axis input is omitted for shell elements.

In addition to plasticity, the deformation sub-model also supports visco-elastic/visco-plastic behavior (see Section 3.1.7) and thermo-mechanical effects (see Section 3.1.9) using additional (optional) user supplied input. The input stress-strain curves are converted into effective stress – effective plastic strain during the pre-processing step and is later used to compute the yield function coefficients during the simulation. These effective stress -effective plastic strain curves cannot have a negative slope (error E 304470 in Table 4.1).

3.1.1 Summary of Required Input

The input required for MAT_213 is in the form of both tabulated data and single point parameters. Table 3.2 shows the input data provided from each experiment. Khaled et al. [2018] provide the experimental methods and post-processing techniques used in the QS-RT testing.

Table 3.2. Required Tests and Resulting Input for MAT_213

Test Description	Resulting Input for MAT_213
Tension 1-direction (T1)	σ_{11}^{T} vs ε_{11}^{T} , $(\varepsilon_{11})_{y}^{T}$, (ν_{12},ν_{13}), $(\nu_{12}^{p},\nu_{13}^{p})$
Tension 2-direction (T2)	σ_{22}^{T} vs ε_{22}^{T} , $(\varepsilon_{22})_{y}^{T}$, (ν_{21},ν_{23}), $(\nu_{21}^{p},\nu_{23}^{p})$
Tension 3-direction (NOT required for shell element) (T3)	σ_{33}^{T} vs ε_{33}^{T} , $(\varepsilon_{33})_{y}^{T}$, (ν_{31},ν_{32}), $(\nu_{31}^{p},\nu_{32}^{p})$
Compression 1-direction (C1)	σ_{11}^{C} vs ε_{11}^{C} , $(\varepsilon_{11})_{y}^{C}$, (ν_{12},ν_{13}), $(\nu_{12}^{p},\nu_{13}^{p})$
Compression 2-direction (C2)	σ_{22}^{C} vs ε_{22}^{C} , $(\varepsilon_{22})_{y}^{C}$, (ν_{21},ν_{23}), $(\nu_{21}^{p},\nu_{23}^{p})$
Compression 3-direction (NOT required for shell element) (C3)	σ_{33}^{C} vs ε_{33}^{C} , $(\varepsilon_{33})_{y}^{C}$, (ν_{31},ν_{32}), $(\nu_{31}^{p},\nu_{32}^{p})$
Shear 1-2 plane (S12)	σ_{12} vs ε_{12} , $(\varepsilon_{12})_{y}$
Shear 2-3 plane (NOT required for shell element) (S23)	σ_{23} vs ε_{23} , $(\varepsilon_{23})_{y}$
Shear 1-3 plane (NOT required for shell element) (S13)	σ_{13} vs ε_{13} , $(\varepsilon_{13})_{y}$
Off-axis tension/compression (45^0, 1-2 plane) (Optional for both shell and solid element) (O12)	σ_{45}^{1-2} vs ε_{45}^{1-2} , $(\varepsilon_{45}^{1-2})_{y}$
Off-axis tension/compression (45^0, 2-3 plane) (NOT required for shell element and optional for solid element) (O23)	σ_{45}^{2-3} vs ε_{45}^{2-3} , $(\varepsilon_{45}^{2-3})_{y}$
Off-axis tension/compression (45^0, 1-3 plane) (NOT required for shell element and optional for solid element) (O13)	σ_{45}^{1-3} vs ε_{45}^{1-3} , $(\varepsilon_{45}^{1-3})_{y}$

3.1.2 Summary Stress-Total Strain Curves

The stress-total strain curves presented in Table 3.2 are in terms of engineering stress-strain except for shear strains that are tensorial quantities. Fig. 3.1 shows the *Model Curves* [Khaled et al., 2017] derived from QS-RT testing of the T800/F3900 composite.

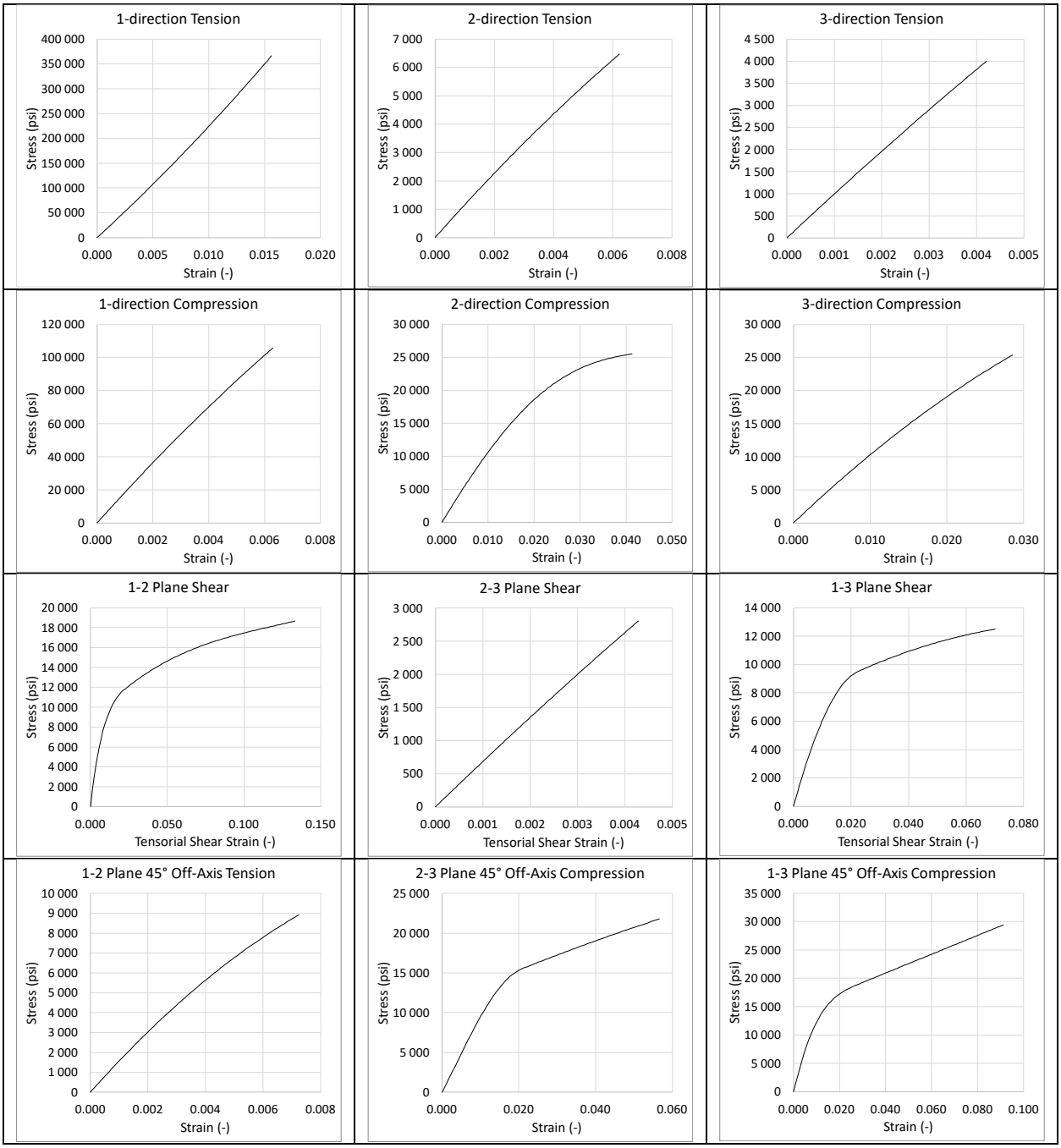

Fig. 3.1. Resulting stress-total strain curves from the twelve tests performed on the T800/F3900 composite under QSRT conditions

Sections 3.1.3 through 3.1.7 show how various parameters are derived directly from the stress-total strain curves shown in Fig. 3.1.

3.1.3 Computation of Yield Strains

The yield strains can be obtained by locating the end of the linear regime of the stress-total strain curve. Fig. 3.2 shows an example using the 2-direction compression curve.

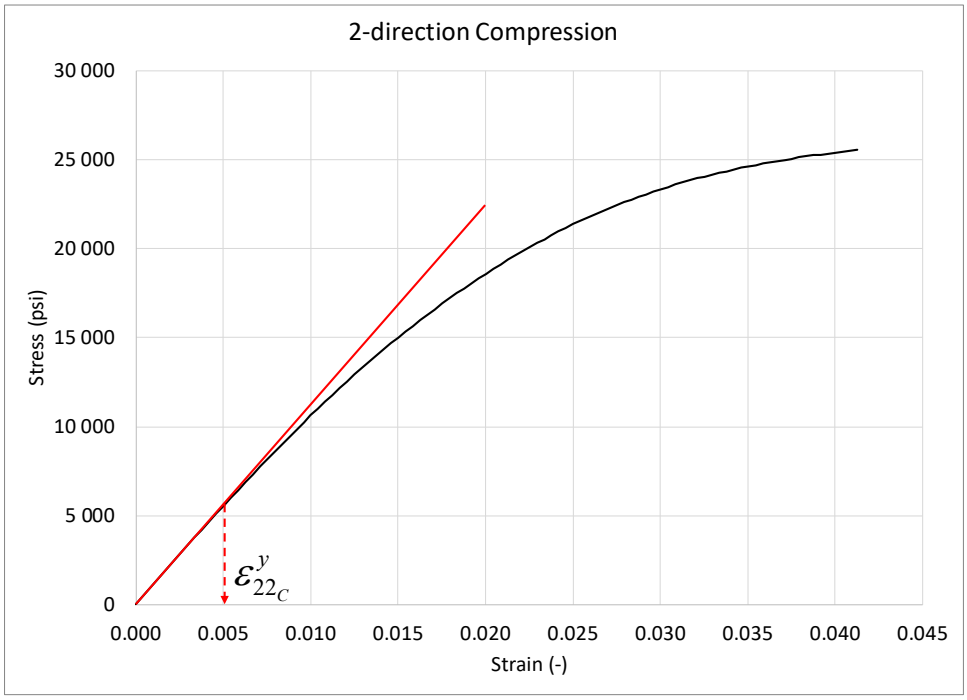

Fig. 3.2. Example of locating the yield strain from the stress-total strain curves

Note 1: The location where linear behavior ends may be subjective since many composites do not exhibit a well-defined yield point. However, if the slope of the curve continues to decrease after the selected yield strain, the material model should not experience any issues during execution. The yield strain corresponding to all the curves are used as input using YSC curve in card 7 of MAT_213 card. Also note that the last two points in a curve are used to extrapolate the curve data when data beyond the end of the user-supplied data is needed.

3.1.4 Computation of Elastic Moduli

After the yield strain has been determined, the Young's modulus and shear modulus can be determined, as shown in Fig. 3.3.

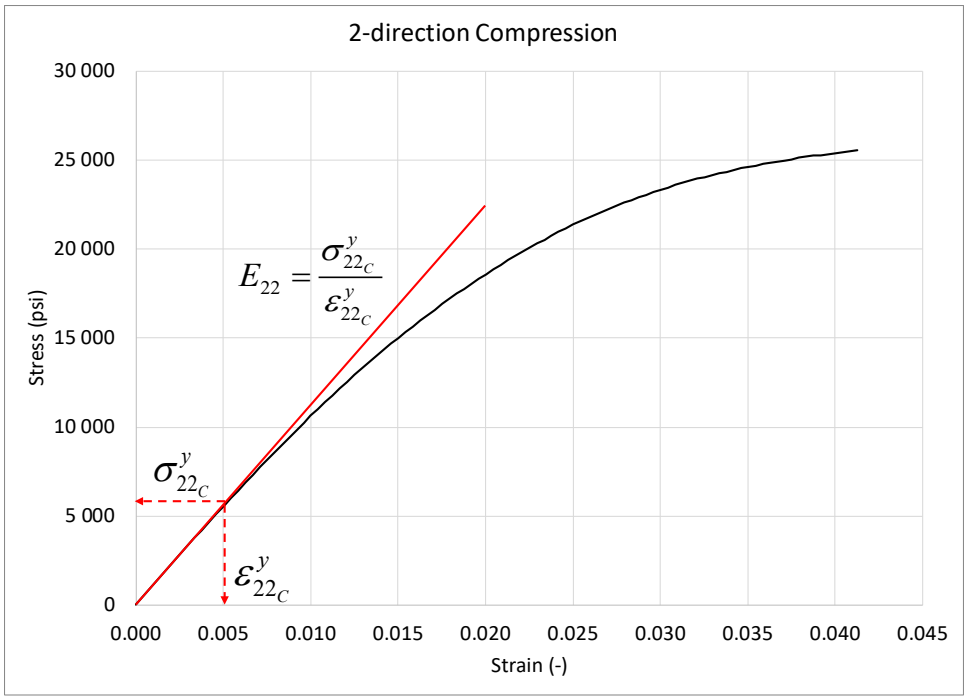

Fig. 3.3. Example of modulus calculation from the stress-total strain curve

Note 2: Computing the moduli externally is required to populate the parameters shown in cards 1 and 2 of the MAT_213 input deck $\left(E_a, E_b, E_c, G_{ab}, G_{bc}, G_{ac}\right)$. MAT_213 dynamically computes and updates the moduli used in the simulation depending on the strain rate and temperature.

3.1.5 Computation of Elastic and Plastic Poisson's Ratios

The elastic and plastic Poisson's ratios can also be computed from the uniaxial tension and compression test data. The elastic Poisson's ratios are input directly to card 1 of the MAT_213 input deck $\left(PR_{ba}, PR_{ca}, PR_{cb}\right)$ while the plastic Poisson's ratios are not. However, the plastic Poisson's ratios are used to compute the required flow rule coefficients $\left(H_{11}, H_{22}, H_{33}, H_{12}, H_{23}, H_{13}, H_{44}, H_{55}, H_{66}\right)$ appearing on cards 5 and 6 of the input deck.

Table 3.3 provides an example of computing the elastic and plastic Poisson's ratios using the 3-direction compression test. Fibers are shown in green in figures where fibers add clarity to the explanations that follow.

Table 3.3. Example of Computing Elastic and Plastic Poisson's Ratio

Step	Visual	Description
1	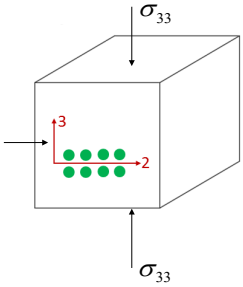 Fig. 3.4. Illustration of test specimen and loading conditions	The specimen is subjected to a state of uniaxial compressive stress in the 3-direction while strains are obtained from the 2-3 plane.
2	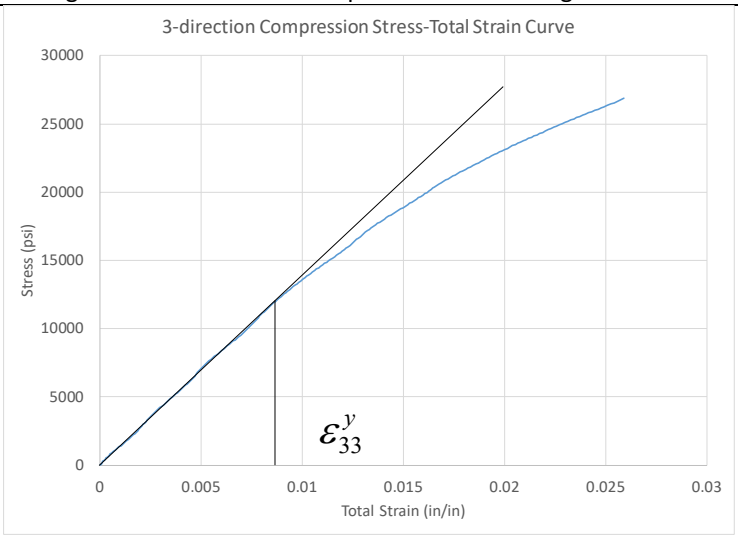 Fig. 3.5. Example of obtaining yield strain	From the longitudinal stress-total strain curve, determine the yield strain (see Fig. 3.5).
3	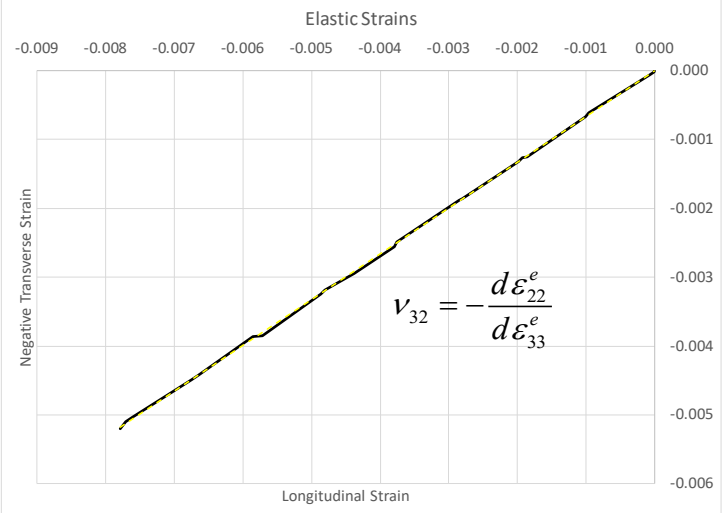 Fig. 3.6. Example of computing elastic Poisson's ratio	All longitudinal and transverse strains before the longitudinal yield strain are assumed to be completely elastic. Compute elastic Poisson's ratio, ν_{32}, as the slope of the regression line through the data (see Fig. 3.6)
4	$Longitudinal: \quad \varepsilon_{33}^{p} = \varepsilon_{33}^{t} - \varepsilon_{33}^{e} = \varepsilon_{33}^{t} - \frac{\sigma_{33}}{E_{33}}$ $Transverse: \quad \varepsilon_{22}^{p} = \varepsilon_{22}^{t} - \varepsilon_{22}^{e} = \varepsilon_{22}^{t} - \nu_{32}\frac{\sigma_{33}}{E_{33}}$	Compute longitudinal and transverse plastic strains after yield strain for all values of stress.

5	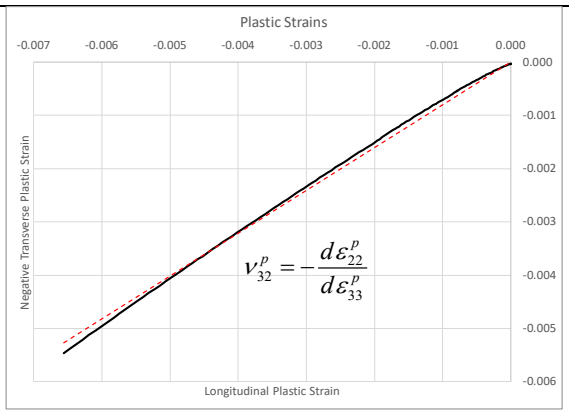 Fig. 3.7. Example of computing plastic Poisson's ratio	Compute plastic Poisson's ratio, ν_{32}^p, as the slope of the regression line through the data (see Fig. 3.7). The slope of the data may not be constant. However, a single value is required, and the average value is an acceptable single value.

3.1.6 Computation of Flow Rule Coefficients

The flow rule coefficients are used to describe the development of plastic strains in the material through the non-associated flow rule as

$$d\boldsymbol{\varepsilon}^p = d\lambda \frac{\partial h}{\partial \boldsymbol{\sigma}} \tag{0.1}$$

h is the plastic potential function and is expressed as

$$\begin{aligned} h^2 = {} & H_{11}\sigma_{11}^2 + H_{22}\sigma_{22}^2 + H_{33}\sigma_{33}^2 + 2H_{12}\sigma_{11}\sigma_{22} + 2H_{23}\sigma_{22}\sigma_{33} + 2H_{13}\sigma_{11}\sigma_{33} \\ & + H_{44}\sigma_{12}^2 + H_{55}\sigma_{23}^2 + H_{66}\sigma_{13}^2 \end{aligned} \tag{0.2}$$

The plastic Poisson's ratios are used to express a subset of the flow rule coefficients:

$$\begin{array}{ccc} 1-2\ Plane & 2-3\ Plane & 1-3\ Plane \\ \nu_{xy}^p\big|_{\theta=0^\circ} = \nu_{12}^p = -\frac{d\varepsilon_{22}^p}{d\varepsilon_{11}^p} = -\frac{H_{12}}{H_{11}} & \nu_{xy}^p\big|_{\theta=0^\circ} = \nu_{23}^p = -\frac{d\varepsilon_{33}^p}{d\varepsilon_{22}^p} = -\frac{H_{23}}{H_{22}} & \nu_{xy}^p\big|_{\theta=0^\circ} = \nu_{13}^p = -\frac{d\varepsilon_{33}^p}{d\varepsilon_{11}^p} = -\frac{H_{13}}{H_{11}} \\ \nu_{xy}^p\big|_{\theta=90^\circ} = \nu_{21}^p = -\frac{d\varepsilon_{11}^p}{d\varepsilon_{22}^p} = -\frac{H_{12}}{H_{22}} & \nu_{xy}^p\big|_{\theta=90^\circ} = \nu_{32}^p = -\frac{d\varepsilon_{22}^p}{d\varepsilon_{33}^p} = -\frac{H_{23}}{H_{33}} & \nu_{xy}^p\big|_{\theta=90^\circ} = \nu_{31}^p = -\frac{d\varepsilon_{11}^p}{d\varepsilon_{33}^p} = -\frac{H_{13}}{H_{33}} \end{array} \tag{0.3}$$

This system of equations is rank deficient and thus does not yield a unique solution. A common solution to this problem is to set one of the coefficients to a value of one, typically one of the values corresponding to the response in PMD (i.e., H_{11}, H_{22}, or H_{33}). For unidirectional composites with the fibers in the 1-direction, the value of H_{22} is often assumed as unity. This assumption leads to the 2-direction tension or compression stress-plastic strain response being the representative effective stress-effective plastic strain (h-λ) response of the material.

However, the choice of the master curve may not be obvious for some composite materials. This section provides details of how the coefficient values can be determined without first assuming a value of one of the coefficients. The example shown is with respect to unidirectional composites but can be applied to any composite architecture provided enough data is available.

First, the plastic potential function (also taken as the effective stress) can be simplified to better represent the plastic flow behavior of unidirectional composites. Plastic strains typically do not develop in the direction aligned with the unidirectional fibers. Using the non-associated flow rule (Eq. (3.1)), the plastic strain in the 1-direction can be written as

$$d\varepsilon_{11}^{p} = \frac{d\lambda}{h}\left(H_{11}\sigma_{11} + H_{12}\sigma_{22} + H_{13}\sigma_{33}\right) \tag{0.4}$$

For the plastic strain in the 1-direction to remain zero for any combination of stresses, the values of H_{11}, H_{12}, and H_{13} must be equal to zero. Additionally, at the lamina level, unidirectional composites exhibit isotropy in the 2-3 plane and hence a simplified version of the plastic potential function can be written as

$$h^2 = H_{22}\left(\sigma_{22}^2 + \sigma_{33}^2\right) + 2H_{23}\sigma_{22}\sigma_{33} + H_{44}\left(\sigma_{12}^2 + \sigma_{13}^2\right) + H_{55}\sigma_{23}^2 \tag{0.5}$$

Under plane stress in the 1-2 plane, the plastic potential function can be further reduced to

$$h^2 = H_{22}\sigma_{22}^2 + H_{44}\sigma_{12}^2 \tag{0.6}$$

Under arbitrary loading in the 1-2 plane, the plastic potential function can be written in terms of the angle of loading with respect to the PMD. Fig. 3.8 shows a specimen where the PMD, shown in the 1-2 plane as an example, are rotated at an arbitrary angle from the longitudinal axis. A stress induced along the X-axis is denoted as σ_x.

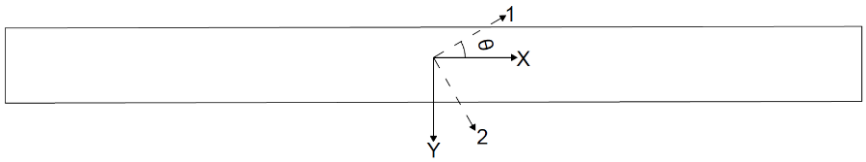

Fig. 3.8. Off-axis tension/compression specimen in the 1-2 plane

The plastic potential function (effective stress) is written as follows

$$h = \sigma_x g\left(\theta\right) \tag{0.7}$$

The plastic multiplier increment (effective plastic strain increment) is given by

$$d\lambda = \frac{d\varepsilon_{xx}^{p}}{g(\theta)} \tag{0.8}$$

where the value of $g(\theta)$ is dependent on the flow rule coefficient values and the rotation of the PMD with respect to the loading axis

$$g(\theta) = \left[H_{22} \sin^4(\theta) + H_{44} \sin^2(\theta) \cos^2(\theta) \right]^{\frac{1}{2}} \tag{0.9}$$

Since the data is derived from monotonically loaded uniaxial specimens, the data is monotonically increasing and Eq. (3.8) may be integrated to give a direct solution for the effective plastic strain (λ)

$$\lambda = \frac{\varepsilon_{xx}^{p}}{g(\theta)} \tag{0.10}$$

The plastic strain in the loading direction is computed as

$$\varepsilon_{xx}^{p} = \varepsilon_{xx}^{tot} - \frac{\sigma_{xx}}{E_{xx}} \tag{0.11}$$

The results of tension or compression tests in the 1-2 plane can be used to determine the values of H_{22} and H_{44}. In the procedure discussed next, the results of θ = 10°, 15°, 30°, 45°, and 90° experimental tension tests were utilized [Hoffarth et al., 2017; Khaled, 2019b]. These curves are referred to as *fitting curves*. The average stress-total strain response (*Model Curve*) from each of the curves is shown in Fig. 3.9.

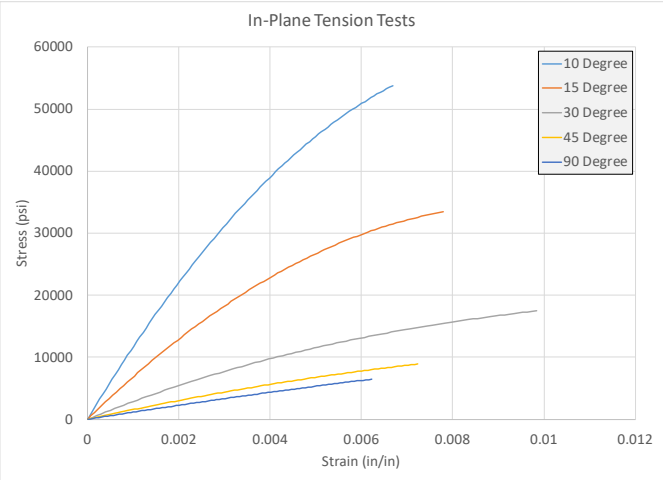

Fig. 3.9. Compilation of 1-2 plane tension stress-total strain curves at off-axis angles of θ = 10°, 15°, 30°, 45°, and 90°

The first step in deriving the values of H_{22} and H_{44}, is converting each of the fitting curves from stress-total strain into stress-plastic strain using Eq. (3.11). Fig. 3.10 shows the resulting curves.

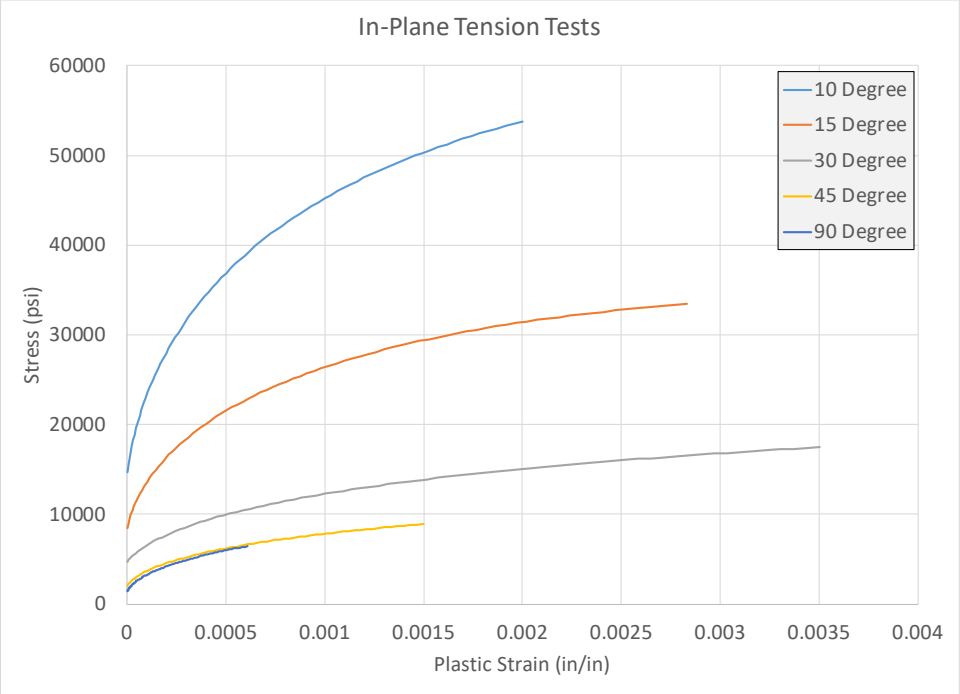

Fig. 3.10. 1-2 plane tension stress-plastic strain curves at off-axis angles of θ = 10°, 15°, 30°, 45°, and 90°

With the assumption that the effective stress (*h*)-effective plastic strain (*λ*) curve is analogous to a composite property, the optimal values of H_{22} and H_{44} will result in the fitting curves collapsing onto a single unique curve in the effective stress-effective plastic strain space. Since there are currently only two degrees of freedom in the equation, H_{22} and H_{44}, an optimization technique can be used to find the optimal values with the only constraint being $H_{ii} \geq 0$. Using the candidate combination of H_{22} and H_{44}, each of the fitting curves is converted into h-λ space using Eq. (3.7) and Eq. (3.10), respectively. From the resulting fitting curves, the average response is computed, $\bar{h}$-*λ*, for the candidate values of H_{22} and H_{44}. At each value of effective plastic strain, λ_j, the average effective stress, $\bar{h}_j$, is computed as

$$\bar{h}_j = \frac{1}{N}\sum_{i=1}^{N} h_i\left(\lambda_j\right) \tag{0.12}$$

where *N* is the number of fitting curves. To determine how far away the current combination of H_{22} and H_{44} are from optimal, the normalized root mean square error (NRMSE) is computed between the fitting curves and the average response as

$$NRMSE = \frac{\sqrt{\frac{1}{N}\sum_{j=1}^{M_i}\sum_{i=1}^{N}\left[h_i(\lambda_j) - \bar{h}(\lambda_j)\right]^2}}{\bar{h}_{\max} - \bar{h}_{\min}} \tag{0.13}$$

where M_i is the number of points along the curves where the computation is performed. The range of effective stress in the average curve is used as the normalizing parameter to provide a consistent frame of reference since the magnitude of the effective stress varies greatly depending on the values of H_{22} and H_{44}. The combination of H_{22} and H_{44} which minimizes the NRMSE is considered the fitted solution. Fig. 3.11 shows a comparison of the fitting curves in h-λ space for a non-fitted combination and a fitted combination.

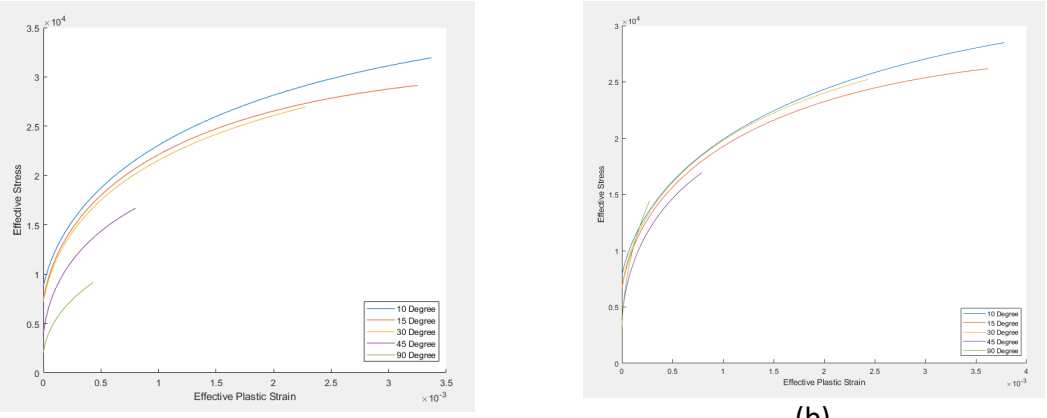

(a) (b)

Fig. 3.11. Fitting curves in h-λ space (a) non-optimal $H_{22} = 2$, $H_{44} = 12$ and (b) optimal $H_{22} = 4.97$, $H_{44} = 9.44$

The fitted combination of H_{22} and H_{44} in Fig. 3.11b may not be unique. Fig. 3.12 shows the NRMSE surface as a function of H_{22} and H_{44} with the computed optimal value denoted by a red circle.

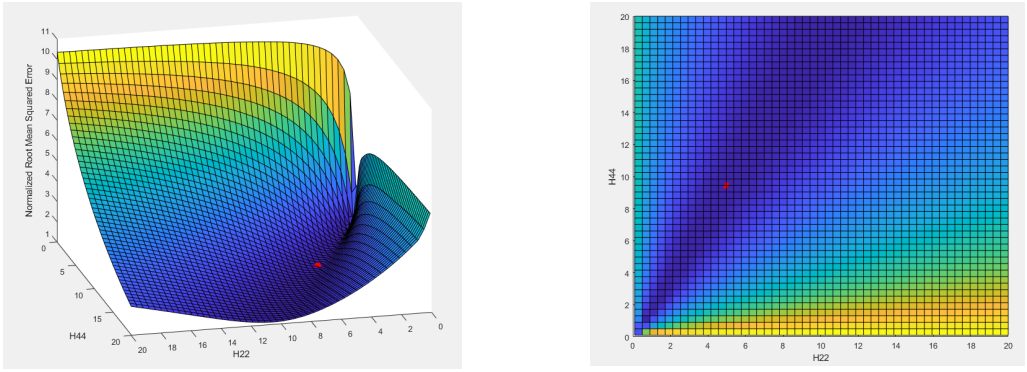

(a) (b)

Fig. 3.12. NRMSE surface (a) three-dimensional view and (b) plan-view

The dark blue region in Fig. 3.12 is a *valley* where the values of NRMSE are approximately equal to the value reported in Fig. 3.11. In fact, all combinations of H_{22} and H_{44} within this region have a nearly constant ratio and each combination is valid for use in MAT_213. The fitted ratio between H_{22} and H_{44} is approximately $\frac{H_{44}}{H_{22}} \cong 1.90$. This result is consistent with the assumption that other researchers have made by taking $H_{22} = 1$, effectively making the 2-direction tension or compression stress-plastic strain curve the master h-λ curve of the material [Sun and Chen, 1989; Ogihara and Reifsnider, 2002].

After computing H_{22} and H_{44}, H_{23} is computed using Eq. (3.3) as

$$H_{23} = -\nu_{23}^{p} H_{22} = -\nu_{32}^{p} H_{33} = -\nu_{32}^{p} H_{22} \tag{0.14}$$

The remaining unknown from Eq. (3.5) is H_{55} which can be computed using the same optimization procedure outlined in this section using the 2-direction tension curve as the master curve and the result from the 2-3 plane 45° off-axis compression test (Fig. 3.1) as the fitting curve. The value of $g(\theta)$, appearing in Eq. (3.7) and Eq. (3.10), changes to

$$g(\theta) = \left[H_{22}\left(\cos^4(\theta) + \sin^4(\theta)\right) + \left(2H_{23} + H_{55}\right)\cos^2(\theta)\sin^2(\theta) \right]^{\frac{1}{2}} \tag{0.15}$$

The methodology can be used to solve for the flow rule coefficients of any composite architecture. The only assumption made was related to the observed linear elastic behavior of the material in the 1-direction, $H_{11} = H_{12} = H_{13} = 0$. This assumption was necessary to preserve the physical admissibility of the resulting coefficients. For other composite architectures, there may be more degrees of freedom during the optimization. However, the process remains similar. Additionally, the choice of utilizing in-plane off-axis tension curves for the initial fitting process is for convenience only. Strictly speaking, the 2-3 plane 45° off-axis compression data could have been used alongside the in-plane curves during the optimization process to solve for H_{55} instead of in a serialized fashion.

The technique presented (referred to herein as the original procedure) is only one of several ways of computing flow rule coefficients for MAT_213. Other techniques may be used to derive the values such that the desired results are obtained. The list below provides a few examples of alternate procedures.

1. The original procedure utilizes data from tests that are not part of the required input for MAT_213 (i.e., tension tests at θ = 10°, 15°, and 30°). However, the additional data is not required, and the same procedure can be performed using only the θ = 45°and θ = 90° curves.

2. The original procedure uses the results of tension tests performed at various loading angles. However, results of compression tests (or both) may also be used to generate the coefficients. Often, compression tests performed on composites provide better insight into the plasticity of the material since ultimate failure happens well after yielding. MAT_213 assumes the plastic flow potential of the composite is the same regardless of whether the stresses induced in the PMDs are tensile or compressive.

3. The original procedure attempts to derive the flow rule coefficients directly from the available experimental data. However, this procedure may not be necessary. Using appropriate numerical calibration, the coefficients can be derived through optimization techniques. For example, a cross-ply tension or compression test where the PMD stresses and plastic strains are different in each layer may be simulated with various values of all flow rule coefficients until the best combination is determined. LS-OPT can be employed to achieve this optimal result. However, when using this approach, the analyst should verify that the values obtained are physically consistent with the input stress-strain curve data. For instance, if the 2-direction exhibits linear elastic behavior, H_{22}, H_{12}, and H_{23} must all be zero, otherwise MAT_213 will encounter errors.

3.1.7 Computation of Viscoelastic Parameters

At this time there is no established process to obtain the values of the decay constants - $\beta_{11}, \beta_{22}, \beta_{33}, \beta_{44}, \beta_{55}, \beta_{66}, \beta_{12}, \beta_{23}$ and β_{13} for use in impact analysis. A suggested approach is to use trial-and-error or an optimization toolbox available in LS-OPT to find the best values for these constants. It should be noted that these parameters are only required if VEVP=1 or 2.

3.1.8 Formatting MAT_213 Input Stress-Total Strain Curves

The entirety of the stress-total strain curves shown in Fig. 3.1 are used as input to MAT_213 and must be organized into "3D table" using functionalities built into LS-DYNA. Fig. 3.13 provides an illustrative schematic of the 3D table structure used in MAT_213 using data from a 1-direction tension test as an example.

<table>
<tr><td rowspan="7">Tension 1-direction</td><td colspan="2">*DEFINE_TABLE_3D
(Temperature)</td><td colspan="2">*DEFINE_TABLE
(Total Strain Rate)</td></tr>
<tr><td rowspan="3">Table 1</td><td rowspan="3">Table 2: 10°C</td><td rowspan="3">Table 2</td><td>Curve 1 (10^{-3}/s)</td></tr>
<tr><td>Curve 2 (1/s)</td></tr>
<tr><td>Curve 3 (10/s)</td></tr>
<tr><td rowspan="3">Table 3: 20°C</td><td rowspan="3">Table 3</td><td>Curve 4 (10^{-3}/s)</td></tr>
<tr><td>Curve 5 (10/s)</td></tr>
</table>

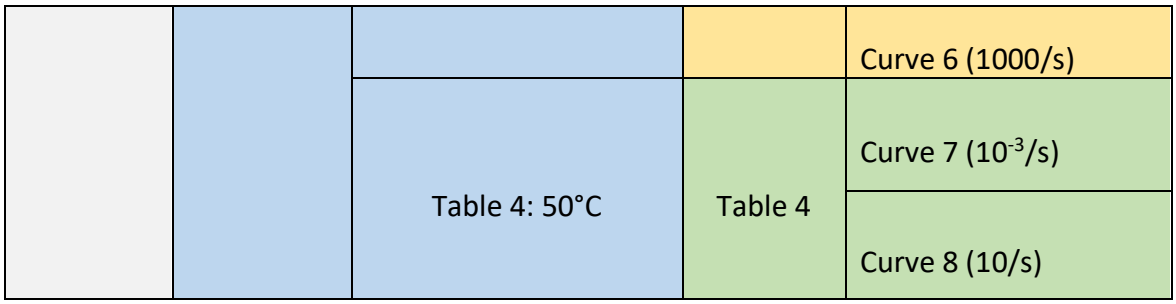

Fig. 3.13. Illustration of the 3D table structure used to define stress-total strain data in MAT_213

The format of the 3D table is as follows:

1. Each experiment type (e.g. tension in the 1-direction, shear in the 2-3 plane) will have a single *DEFINE_TABLE_3D definition for a total of twelve.

2. Each *DEFINE_TABLE_3D definition includes a set of temperatures and their corresponding *DEFINE_TABLE definition (see below).

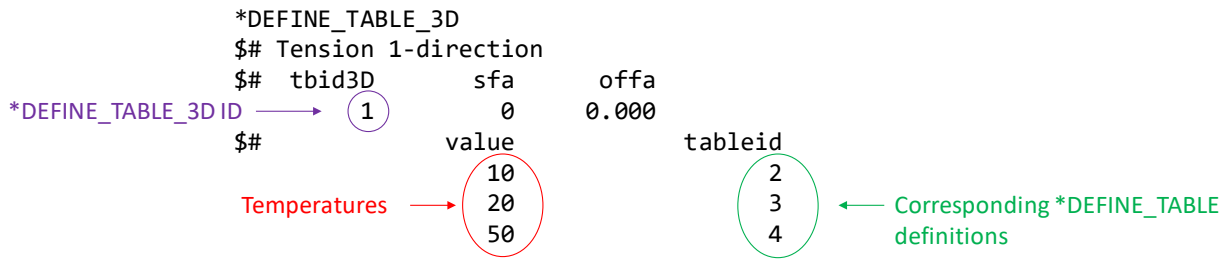

3. Each *DEFINE_TABLE definition contains the strain rates for the given temperature. The stress-total strain curve IDs corresponding to the current strain rate temperature combination are not included in the *DEFINE_TABLE definition (see below).

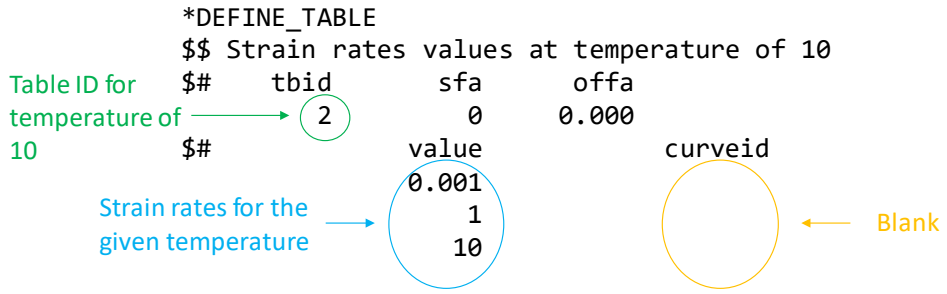

4. Immediately following the end of the definition of the *DEFINE_TABLE definition, the curves corresponding to the strain rates for the given temperature are defined in the same order as what is provided in the *DEFINE_TABLE definition (see below).

```
*DEFINE_CURVE
$$ Stress Strain Curve for temperature of 10 and strain rate of 0.001
$#    lcid      sidr       sfa       sfo      offa      offo    dattyp
         1         0     0.000     0.000     0.000     0.000         0
$#                a1                  o1
            strain_1           stress_1
                   .                  .
                   .                  .
            strain_n           stress_n
*DEFINE_CURVE
$$ Stress Strain Curve for temperature of 10 and strain rate of 1
$#    lcid      sidr       sfa       sfo      offa      offo    dattyp
         2         0     0.000     0.000     0.000     0.000         0
$#                a1                  o1
            strain_1           stress_1
                   .                  .
                   .                  .
            strain_n           stress_n
*DEFINE_CURVE
$$ Stress Strain Curve for temperature of 10 and strain rate of 10
$#    lcid      sidr       sfa       sfo      offa      offo    dattyp
         3         0     0.000     0.000     0.000     0.000         0
$#                a1                  o1
            strain_1           stress_1
                   .                  .
                   .                  .
            strain_n           stress_n
```

First curve following *DEFINE_TABLE definition. Strain rate of 0.001/s.

Second curve following *DEFINE_TABLE definition. Strain rate of 1/s.

Third curve following *DEFINE_TABLE definition. Strain rate of 10/s.

5. Even if there is only one temperature and strain rate combination, (e.g., if only QS-RT data is available), two different strain rates for the given temperature must still be provided in the *DEFINE_TABLE definition. Consequently, two stress-total strain curves must be defined even if the data are identical.

Note 3: The values shown in Fig. 3.13 are only examples; there may be data available at only one temperature or more than three strain rates. There is currently no limitation on the number of strain rate and temperature combinations that may be used as input.

Note 4: As shown in Fig. 3.13, there is no stipulation that requires stress-strain data be defined at the same strain rates for each temperature. Defining the same number of strain rates for each temperature is also not required.

3.1.9 Thermo-mechanical effect

The rise in temperature due to plastic work is given by the following equation,

$$\Delta T = \frac{\beta_t}{c_p \rho} h \Delta \lambda \tag{0.16}$$

where, β_t is the Taylor-Quinney Coefficient [Shyamsunder et al., 2019] which is required as input (TQC in card 11) and c_p is the specific heat (cp in card 11). These two parameters are required as

input for the thermal effects. The reference temperature that is in the input deck is updated with the change in temperature computed using Eq. 3.16.

3.2 Damage Sub-Model

Like the plasticity-based deformation sub-model, the damage sub-model is driven by a set of tabulated damage parameter-total strain curves. However, the damage-related input is optional. The input (damage parameters, see Table 3.4) are used to capture the degradation of the mechanical properties of the composite as the stress or strain in the material intensifies. Within MAT_213, this manifests as a reduction in the load carrying capacity of the composite in a given PMD or PMP.

The damage sub-model can affect the stress-strain response in two ways. First, the elastic stiffness may be reduced during unloading/reloading events prior to failure of the material. Second, softening may be captured following failure of the material. This process can be achieved by inputting appropriate stress-total strain and damage-parameter-total strain curves to MAT_213. Since the deformation and damage sub-models interact with each other during both the initial preprocessing stages and during the actual simulation within MAT_213, the input data must be physically consistent [Shyamsunder et al., 2020c].

The following sections provide details of the available input data, examples of experiments used in deriving the damage parameters, how the data must be formatted, and how the deformation and damage sub-models interact with one each other.

3.2.1 Summary of Possible Input

The input for the damage model consists of a set of tabulated damage parameter-total strain curves. The damage parameter is represented as d_{kl}^{ij} where ij is the direction in which the damage is induced, and kl is the loading direction (causing the damage). If ij and kl are the same, the damage parameter is called uncoupled damage; otherwise it is called coupled damage. MAT_213 has provisions to handle a total of 84 distinct damage parameters. Any combination of the available damage parameters may be used as input; the user is limited only by available data. Of the 84 available parameters, 12 correspond to uncoupled damage and the remainder correspond to coupled damage. There are currently no capabilities to handle either temperature dependent or strain rate dependent damage. Therefore, the same damage parameters are utilized during the simulation irrespective of the strain rate or temperature at a given instance of time. Table 3.4 below provides a summary of the damage parameters available in MAT_213.

Table 3.4. List of Available MAT_213 Damage Parameters and Associated ID Numbers

Parameter ID	Damage Parameter	Parameter ID	Damage Parameter	Parameter ID	Damage Parameter
1	$d_{11_T}^{11_T}\left(\varepsilon_{11_T}\right)$	29	$d_{33_T}^{11_T}\left(\varepsilon_{33_T}\right)$	57	$d_{33_C}^{22_C}\left(\varepsilon_{33_C}\right)$

2	$d_{22_T}^{22_T}\left(\varepsilon_{22_T}\right)$	30	$d_{33_T}^{22_T}\left(\varepsilon_{33_T}\right)$	58	$d_{33_C}^{12}\left(\varepsilon_{33_C}\right)$
3	$d_{33_T}^{33_T}\left(\varepsilon_{33_T}\right)$	31	$d_{33_T}^{11_C}\left(\varepsilon_{33_T}\right)$	59	$d_{33_C}^{23}\left(\varepsilon_{33_C}\right)$
4	$d_{11_C}^{11_C}\left(\varepsilon_{11_C}\right)$	32	$d_{33_T}^{22_C}\left(\varepsilon_{33_T}\right)$	60	$d_{33_C}^{13}\left(\varepsilon_{33_C}\right)$
5	$d_{22_C}^{22_C}\left(\varepsilon_{22_C}\right)$	33	$d_{33_T}^{33_C}\left(\varepsilon_{33_T}\right)$	61	$d_{12}^{11_T}\left(\varepsilon_{12}\right)$
6	$d_{33_C}^{33_C}\left(\varepsilon_{33_C}\right)$	34	$d_{33_T}^{12}\left(\varepsilon_{33_T}\right)$	62	$d_{12}^{22_T}\left(\varepsilon_{12}\right)$
7	$d_{12}^{12}\left(\varepsilon_{12}\right)$	35	$d_{33_T}^{23}\left(\varepsilon_{33_T}\right)$	63	$d_{12}^{33_T}\left(\varepsilon_{12}\right)$
8	$d_{23}^{23}\left(\varepsilon_{23}\right)$	36	$d_{33_T}^{13}\left(\varepsilon_{33_T}\right)$	64	$d_{12}^{11_C}\left(\varepsilon_{12}\right)$
9	$d_{13}^{13}\left(\varepsilon_{13}\right)$	37	$d_{11_C}^{11_T}\left(\varepsilon_{11_C}\right)$	65	$d_{12}^{22_C}\left(\varepsilon_{12}\right)$
10	$d_{O12}^{O12}\left(\varepsilon_{O12}\right)$	38	$d_{11_C}^{22_T}\left(\varepsilon_{11_C}\right)$	66	$d_{12}^{33_C}\left(\varepsilon_{12}\right)$
11	$d_{O23}^{O23}\left(\varepsilon_{O23}\right)$	39	$d_{11_C}^{33_T}\left(\varepsilon_{11_C}\right)$	67	$d_{12}^{23}\left(\varepsilon_{12}\right)$
12	$d_{O13}^{O13}\left(\varepsilon_{O13}\right)$	40	$d_{11_C}^{22_C}\left(\varepsilon_{11_C}\right)$	68	$d_{12}^{13}\left(\varepsilon_{12}\right)$
13	$d_{11_T}^{22_T}\left(\varepsilon_{11_T}\right)$	41	$d_{11_C}^{33_C}\left(\varepsilon_{11_C}\right)$	69	$d_{23}^{11_T}\left(\varepsilon_{23}\right)$
14	$d_{11_T}^{33_T}\left(\varepsilon_{11_T}\right)$	42	$d_{11_C}^{12}\left(\varepsilon_{11_C}\right)$	70	$d_{23}^{22_T}\left(\varepsilon_{23}\right)$
15	$d_{11_T}^{11_C}\left(\varepsilon_{11_T}\right)$	43	$d_{11_C}^{23}\left(\varepsilon_{11_C}\right)$	71	$d_{23}^{33_T}\left(\varepsilon_{23}\right)$
16	$d_{11_T}^{22_C}\left(\varepsilon_{11_T}\right)$	44	$d_{11_C}^{13}\left(\varepsilon_{11_C}\right)$	72	$d_{23}^{11_C}\left(\varepsilon_{23}\right)$
17	$d_{11_T}^{33_C}\left(\varepsilon_{11_T}\right)$	45	$d_{22_C}^{11_T}\left(\varepsilon_{22_C}\right)$	73	$d_{23}^{22_C}\left(\varepsilon_{23}\right)$
18	$d_{11_T}^{12}\left(\varepsilon_{11_T}\right)$	46	$d_{22_C}^{22_T}\left(\varepsilon_{22_C}\right)$	74	$d_{23}^{33_C}\left(\varepsilon_{23}\right)$
19	$d_{11_T}^{23}\left(\varepsilon_{11_T}\right)$	47	$d_{22_C}^{33_T}\left(\varepsilon_{22_C}\right)$	75	$d_{23}^{12}\left(\varepsilon_{23}\right)$
20	$d_{11_T}^{13}\left(\varepsilon_{11_T}\right)$	48	$d_{22_C}^{11_C}\left(\varepsilon_{22_C}\right)$	76	$d_{23}^{13}\left(\varepsilon_{23}\right)$
21	$d_{22_T}^{11_T}\left(\varepsilon_{22_T}\right)$	49	$d_{22_C}^{33_C}\left(\varepsilon_{22_C}\right)$	77	$d_{13}^{11_T}\left(\varepsilon_{13}\right)$
22	$d_{22_T}^{33_T}\left(\varepsilon_{22_T}\right)$	50	$d_{22_C}^{12}\left(\varepsilon_{22_C}\right)$	78	$d_{13}^{22_T}\left(\varepsilon_{13}\right)$
23	$d_{22_T}^{11_C}\left(\varepsilon_{22_T}\right)$	51	$d_{22_C}^{23}\left(\varepsilon_{22_C}\right)$	79	$d_{13}^{33_T}\left(\varepsilon_{13}\right)$
24	$d_{22_T}^{22_C}\left(\varepsilon_{22_T}\right)$	52	$d_{22_C}^{13}\left(\varepsilon_{22_C}\right)$	80	$d_{13}^{11_C}\left(\varepsilon_{13}\right)$
25	$d_{22_T}^{33_C}\left(\varepsilon_{22_T}\right)$	53	$d_{33_C}^{11_T}\left(\varepsilon_{33_C}\right)$	81	$d_{13}^{22_C}\left(\varepsilon_{13}\right)$
26	$d_{22_T}^{12}\left(\varepsilon_{22_T}\right)$	54	$d_{33_C}^{22_T}\left(\varepsilon_{33_C}\right)$	82	$d_{13}^{33_C}\left(\varepsilon_{13}\right)$
27	$d_{22_T}^{23}\left(\varepsilon_{22_T}\right)$	55	$d_{33_C}^{33_T}\left(\varepsilon_{33_C}\right)$	83	$d_{13}^{12}\left(\varepsilon_{13}\right)$
28	$d_{22_T}^{13}\left(\varepsilon_{22_T}\right)$	56	$d_{33_C}^{11_C}\left(\varepsilon_{33_C}\right)$	84	$d_{13}^{23}\left(\varepsilon_{13}\right)$

3.2.2 Computation of Damage Parameters

The input data required to drive the damage sub-model is in the form of damage parameter-total strain curves. The data is used to describe the damage that the specimen incurs under monotonic loading. However, the data may be obtained from a series of cyclic loading curves. The assumption is that no additional damage is induced in the specimen during the elastic unloading/reloading cycles.

While MAT_213 allows for up to 84 damage parameters to be utilized, in most cases, experimentally characterizing all of them is unnecessary. For example, the monotonic stress-total strain curves presented in Fig. 3.1 shows only a subset of the PMD or PMP, exhibiting significant nonlinearity under uniaxial monotonic loading: 2-direction compression, 1-2 plane shear, and 1-3 plane shear. A portion of the nonlinearity is likely due to the manifestation of damage in the composite material. Table 3.5 shows which damage parameters have been derived for the T800/F3900 composite [Khaled et al., 2017b].

Table 3.5. Damage Parameters Characterized for the T800/F3900 Composite

Test name and parameter	**Description**
Uncoupled 2-direction compression $\left(d_{22_C}^{22_C}\right)$	Load specimen in 2-direction in compression, then interrogate specimen in elastic regime in 2-direction in compression.
Uncoupled 1-2 plane shear $\left(d_{12}^{12}\right)$	Load specimen in 1-2 plane in shear, then interrogate specimen in elastic regime in 1-2 plane in shear.
Coupled 2-direction compression 2-direction tension $\left(d_{22_C}^{22_T}\right)$	Load specimen in 2-direction in compression, then interrogate specimen in elastic regime in 2-direction in tension.
Coupled 2-direction compression 1-2 plane shear $\left(d_{22_C}^{12}\right)$	Load specimen in 2-direction in compression, then interrogate specimen in elastic regime in 1-2 plane in shear.

Table 3.5 shows both uncoupled and coupled damage parameters. The distinct experimental procedures used to derive the parameters are described below.

In general, the procedures involve loading a specimen in a certain direction into the nonlinear regime, the onset of which is determined from monotonic testing conducted earlier. After loading the specimen into the nonlinear regime (i.e., initial state to point 1 in Fig. 3.14a and Fig. 3.14b), it is unloaded to a stress-free state (i.e., point 1 to point 2 in Fig. 3.14 and Fig. 3.14b), and subsequently loaded elastically in the direction of interest. During the elastic loading cycle, three additional conditioning cycles are performed, for example, from point 2 to point 1a in Fig. 3.14a and Fig. 3.14c. The conditioning cycles yield multiple measurements of the elastic stiffness at the same level of damage so that one can differentiate between reduction in stiffness and

experimental error. Fig. 3.14 shows how the uncoupled and coupled experimental procedures work.

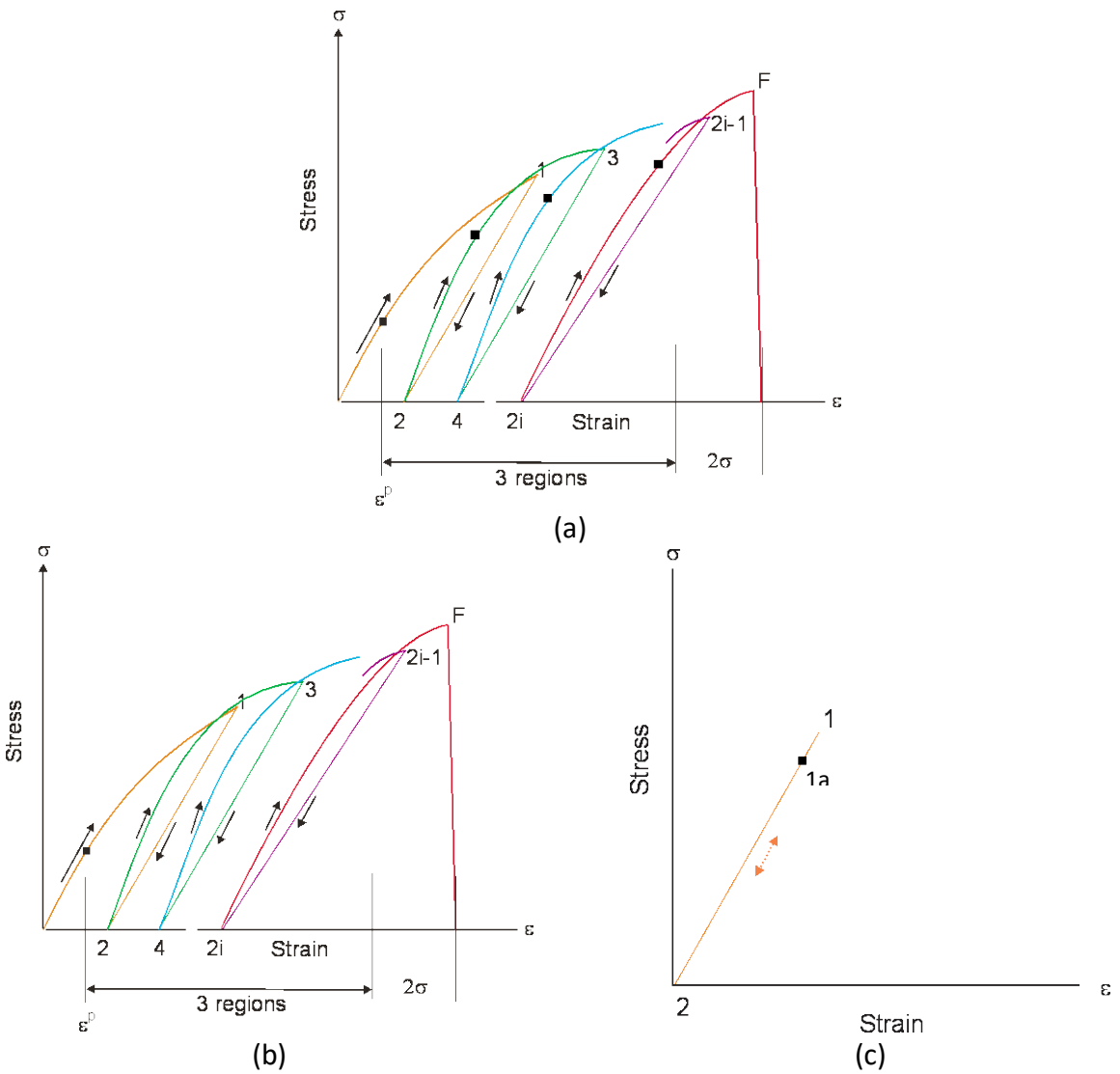

Fig. 3.14. Illustration of Experimental Procedure for (a) Uncoupled Damage Tests and (b), (c) Coupled Damage Tests

After performing the cyclic loading experiments, the damaged modulus must be computed corresponding to the value of strain at each point of unload, e.g. points 1 and 3 in Fig. 3.14a and Fig. 3.14b.The reduced moduli can be computed using various methods, two of which have been employed to reduce the T800/F3900 data. The first is to perform a linear regression on the loading or unloading path during the interrogation cycles, illustrated by the dashed lines in Fig. 3.15b. The slope of the regression model is taken as the modulus and the values for all load and unload conditioning cycles, at the current value of strain shown by the red dot in Fig. 3.15a, are averaged. The average slope is taken as the modulus corresponding to the current level of damage.

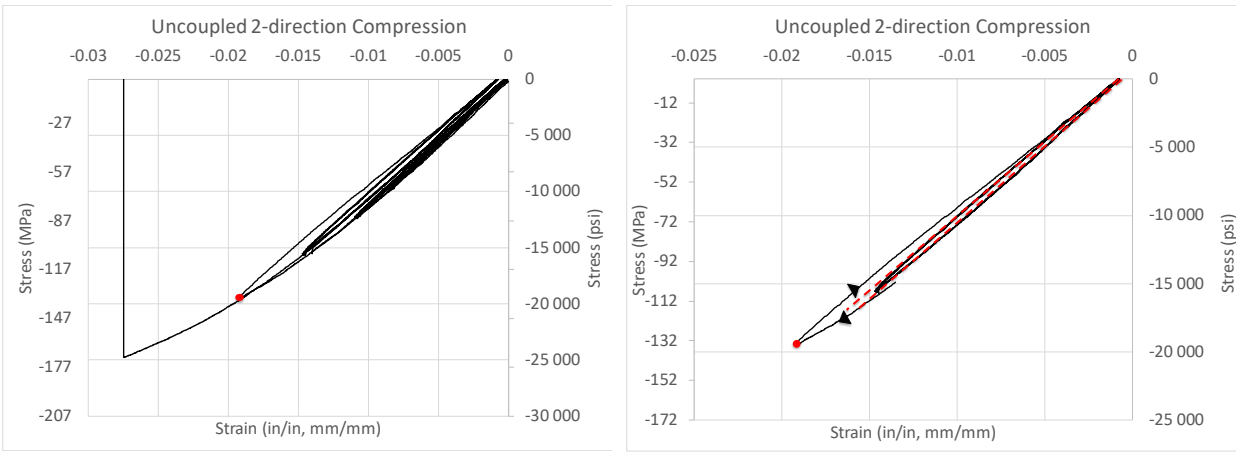

(a) (b)

Fig. 3.15. General Procedure Used to Determine Reduced Modulus with Mostly Linear Load/Unload Behavior (a) Full Experimental Curve and (b) One Cycle Isolated

Fig. 3.16 illustrates an alternative technique that is used when the hysteresis loops become large and the load/unload path is highly nonlinear making it difficult to choose the region to perform the linear regression. In this case, an average slope is used which corresponds to the line between the point where unloading is initiated and the point corresponding to the stress-free state.

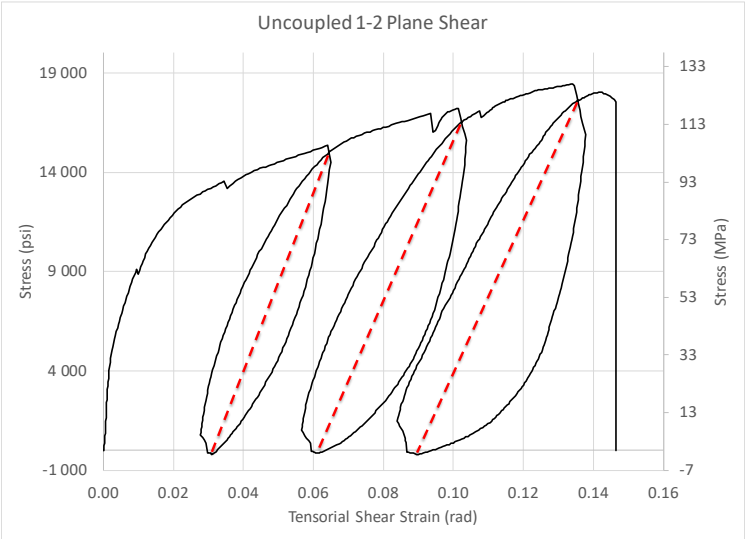

Fig. 3.16. General Procedure Used to Determine Reduced Modulus with Large Hysteretic Loops

The hysteretic behavior shown in Fig. 3.16 is not captured in the constitutive model as only linear elastic unloading behavior is considered. The damage parameters can be computed as

$$d\left(\varepsilon_i^t\right) = 1 - \frac{E\left(\varepsilon_i^t\right)}{E\left(\varepsilon_0^t\right)} \tag{0.17}$$

where $d\left(\varepsilon_i^t\right)$ is the damage parameter corresponding to the total strain at unload point *i*, $E\left(\varepsilon_i^t\right)$ is the elastic stiffness corresponding to unload point *i*, and $E\left(\varepsilon_0^t\right)$ is the elastic stiffness corresponding to the undamaged specimen. After computing the damage parameter corresponding to all unload points, a damage-total strain curve is generated. The damage values begin at the initial plastic strain value corresponding to the direction in which damage is induced and ends at the final strain value of the corresponding monotonic curve of the direction in which damage is induced. Data can be extrapolated to the initial plastic strain value and final strain value using curve fitting techniques. Fig. 3.17 shows an example of the damage parameter-total strain input curve using data from the uncoupled 1-2 plane shear damage tests.

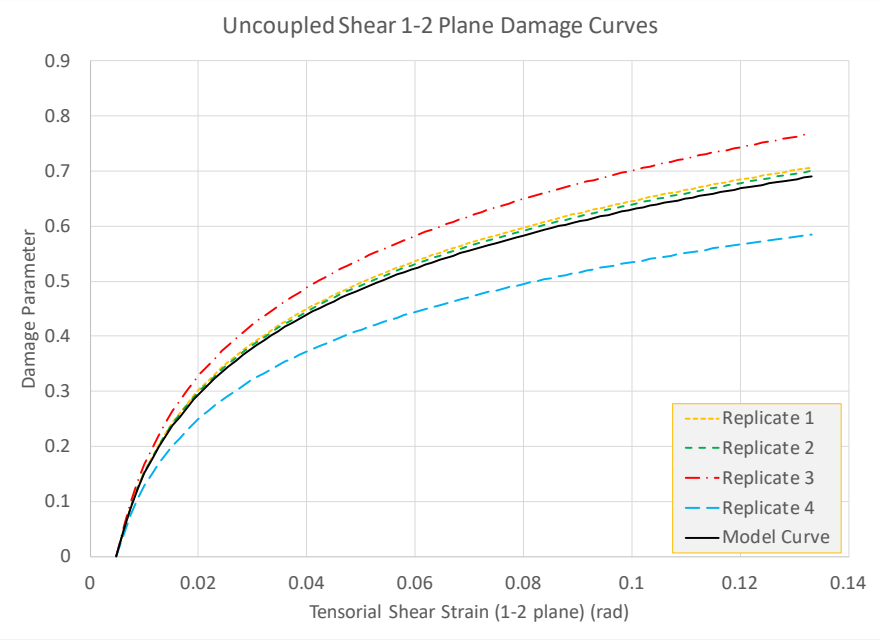

Fig. 3.17. Damage parameter-total tensorial shear strain curves for uncoupled 1-2 plane shear tests $\left(d_{12}^{12}\right)$

The *Model Curve* shown in Fig. 3.17 is the average of the experimental data and is used as the input to MAT_213.

3.2.3 Consistency between Deformation Sub-Model and Damage Sub-Model

During both the pre-processing and execution stages of MAT_213, the deformation and damage sub-models interact with each other. As such, there are provisions that must be made when formatting the input data for both models respectively to ensure that resulting behavior remains physically admissible. Many of the possible inconsistencies are caught by MAT_213, but the onus is on the user to adjust the input data if there are inconsistencies. Most issues arise when the upper limit of damage, at a given point on the corresponding input stress-total strain curve, is violated. Negative plastic strains are computed when this occurs resulting in an error during the

preprocessing stage. The equation below shows the way plastic strains are computed during the pre-processing stage.

$$\varepsilon_{ij}^{p}\left(\varepsilon_{ij}^{t}\right)=\varepsilon_{ij}^{t}-\frac{\sigma_{ij}\left(\varepsilon_{ij}^{t}\right)}{\left(1-d_{ij}^{ij}\left(\varepsilon_{ij}^{t}\right)\right)E_{ij}} \tag{0.18}$$

where ε_{ij}^{t} is the total strain at the point of interest on the input stress-total strain curve, ε_{ij}^{p} is the plastic strain corresponding to a value of the original total strain, σ_{ij} is the true stress corresponding to a value of the original total strain, d_{ij}^{ij} is the uncoupled damage parameter corresponding to the stress-total strain curve being processed, and E_{ij} is the undamaged Young's modulus in direction *ij*. In the case of shear curves, E_{ij} is replaced with $2G_{ij}$ since the input is assumed to be in terms of tensorial shear strain. Eq. (3.18) represents the first portion of the pre-processing stage where the input stress-total strain curves (Fig. 3.1) are converted into stress-plastic strain curves. Only uncoupled damage parameters $\left(d_{ij}^{ij}\left(\varepsilon_{ij}^{t}\right)\right)$ are used since during the monotonic test, it is assumed that only uncoupled damage has manifested itself in the true stress-total strain response. The minimum admissible value of plastic strain is 0. Thus Eq. (3.18) may be rearranged to yield the largest value of the uncoupled damage parameter for a given point on the stress-total strain curve as

$$\left[d_{ij}^{ij}\left(\varepsilon_{ij}^{t}\right)\right]_{\max}=1-\frac{\sigma_{ij}\left(\varepsilon_{ij}^{t}\right)}{E_{ij}\varepsilon_{ij}^{t}} \tag{0.19}$$

Fig. 3.18 shows the resulting effective stress-plastic strain curve when inconsistent data is utilized (note plastic strains become negative with inconsistent data). This data is used during the simulation to obtain yield stresses for the plasticity-based deformation sub-model.

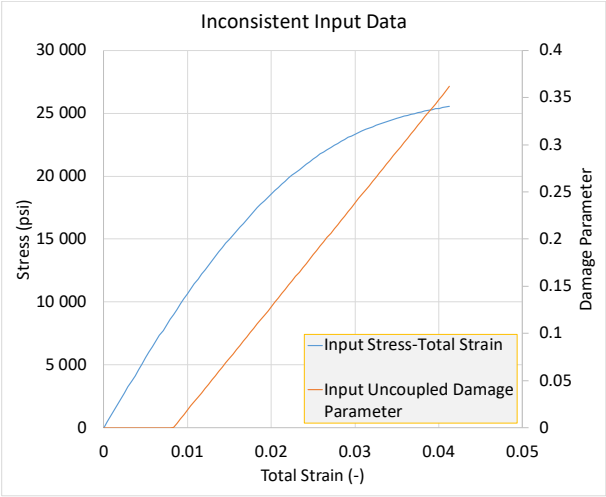

(a)

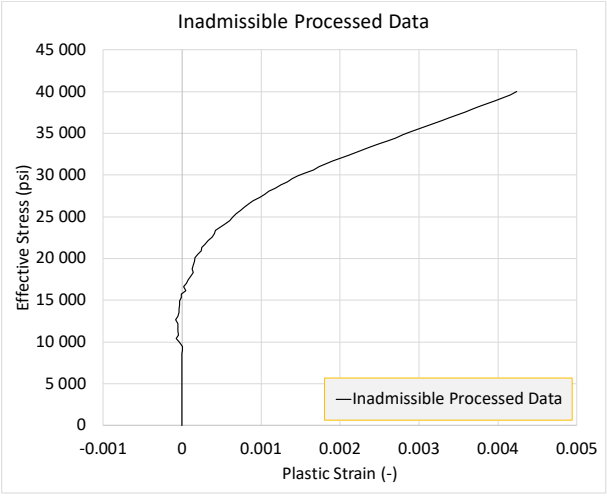

(b)

Fig. 3.18. Examples of data which result in inconsistencies between the damage sub-model and deformation sub-model (a) Input stress-total strain data and related uncoupled damage parameter and (b) Resulting inadmissible effective stress-plastic strain curve used in plasticity algorithm

Fig. 3.18 shows the effect of damage parameters on the stress-strain response prior to failure. However, damage can also be used to define strain softening provided the admissibility conditions are satisfied. Fig. 3.19 shows an example of how strain softening can be captured using the 1-2 plane shear response as an example.

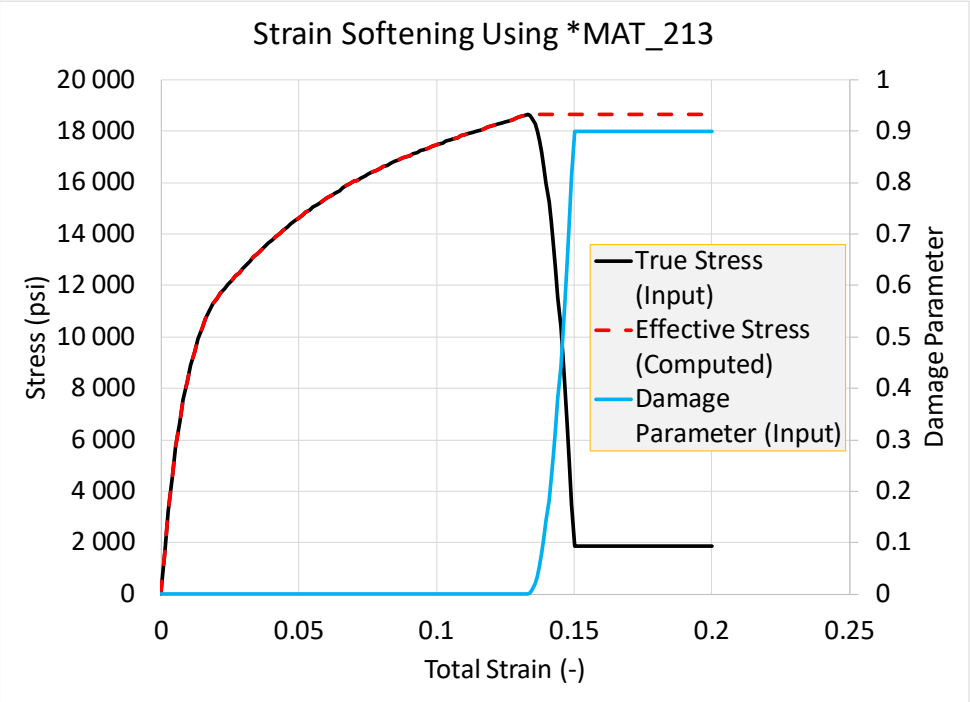

Fig. 3.19. Example of how to capture strain softening behavior using available MAT_213 input parameters

In Fig. 3.19, the *True Stress* curve represents an example of the desired 1-2 plane shear behavior. This behavior cannot be simulated using only the deformation sub-model since the negative slope in the post-peak region would violate stability conditions in the plasticity algorithm. Using the corresponding uncoupled damage parameter to reduce the stress capacity of the material, in this case $d_{12}^{12}\left(\varepsilon_{12}\right)$, labeled *Damage Parameter* in Fig. 3.19, a physically admissible effective stress can be generated during the pre-processing stage of MAT_213. Since the effective stress is used in plasticity computations, the input combination shown does not cause any issues during execution of MAT_213. The combination of damage parameter and true stress can be altered to yield the desired response as long as the effective stress has a constant or increasing value (slope of the effective stress vs total strain/plastic strain/effective plastic strain curve does not become negative).

3.2.4 Formatting MAT_213 Input Damage Parameter-Total Strain Curves

Like the deformation sub-model, the entirety of the damage parameter data must be organized into a set of curves. It should be noted that damage data can berate and temperature dependent and are used with all relevant input stress-strain curves in MAT_213 V1.3.6 and later versions.

a) Example 1: Temperature and strain-rate independent damage curves - To include temperature and strain- rate independent damage information for $d_{bb_C}^{bb_C}(\varepsilon_{bb_C})$ (uncoupled b-direction compression), $d_{ab}^{ab}(\varepsilon_{ab})$ (uncoupled shear a-b), $d_{bb_C}^{bb_T}(\varepsilon_{bb_C})$ (coupled b-direction compression and b-direction tension) and $d_{bbC}^{ab}(\varepsilon_{bb_C})$ (coupled b-direction compression and $a-b$ direction shear) the following input can be used.

1. Define the "DC" in the MAT_213 input deck (Chapter 3). This value corresponds to the *DEFINE_CURVE curve ID containing the damage parameter IDs (Table 3.4) and their corresponding *DEFINE_CURVE curve IDs.

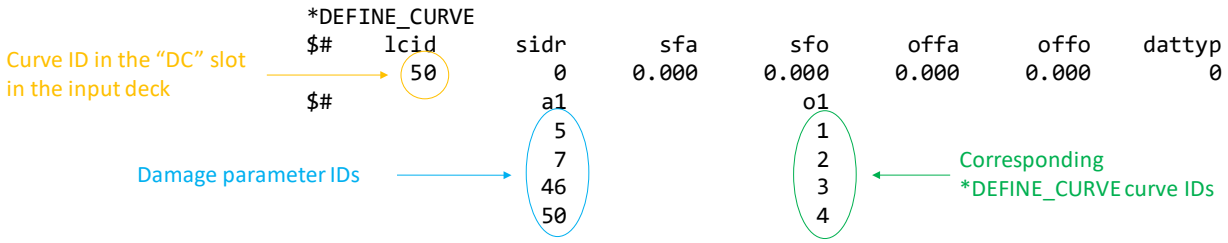

Note 5: Only active damage parameters need to be included in the input.

2. Each of the *DEFINE_CURVE curve IDs correspond to curves containing tabulated total strain-damage parameter data for each of the active damage parameters.

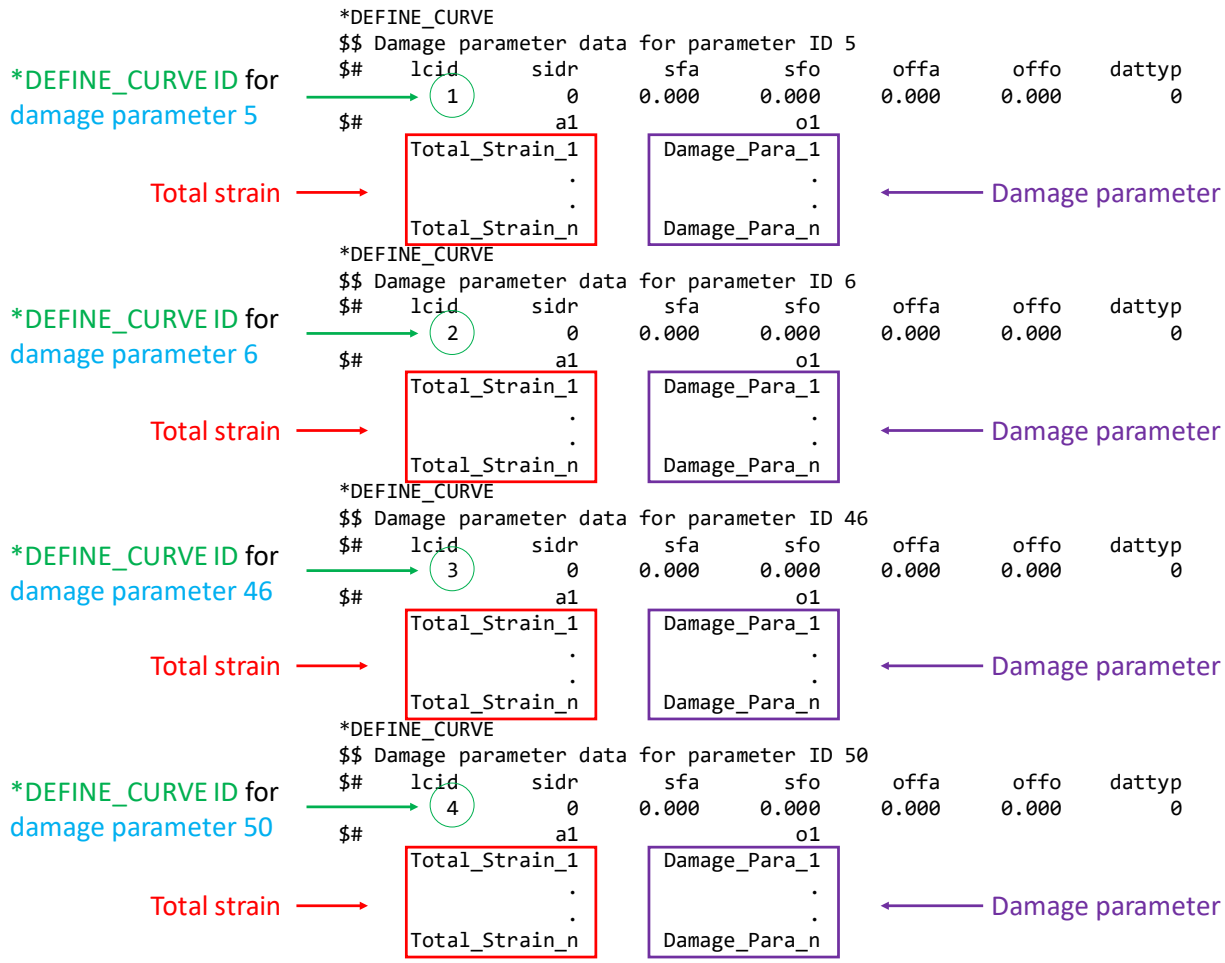

b) ***Example for rate and temperature dependent damage data*** - To include damage information for three different strain rates (0.0001/s, 0.001/s and 325/s) at temperature 36℃ for $d_{bb_T}^{bb_T}(\varepsilon_{bb_T})$ (uncoupled b-direction tension) only, the following input cards can be used.

1. Define the "DC" in the MAT_213 input deck (Chapter 3). This value corresponds to the *DEFINE_CURVE curve ID containing the damage parameter IDs (Table 3.4) and their corresponding *DEFINE_Table_3D IDs for temperature dependent damage (see below).

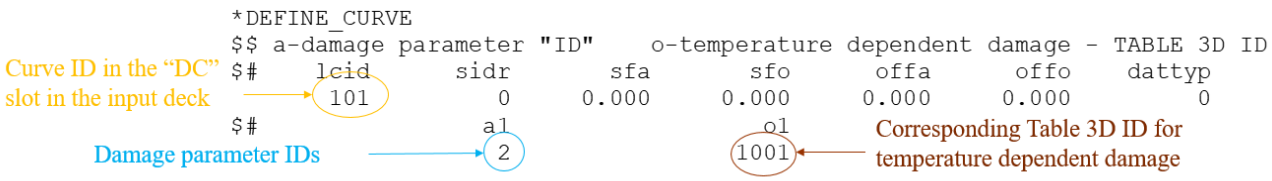

2. Each DEFINE_Table_3D ID includes a set of temperature values and their corresponding *DEFINE_Table IDs for different strain rates (see below).

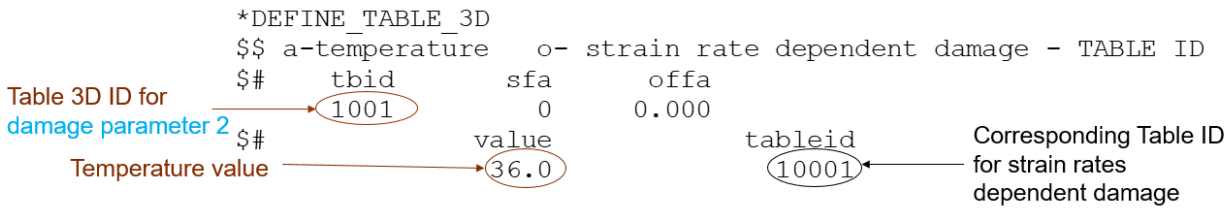

3. Each *DEFINE_Table ID includes a set of strain rates and corresponding *DEFINE_CURVE curve IDs (see below).

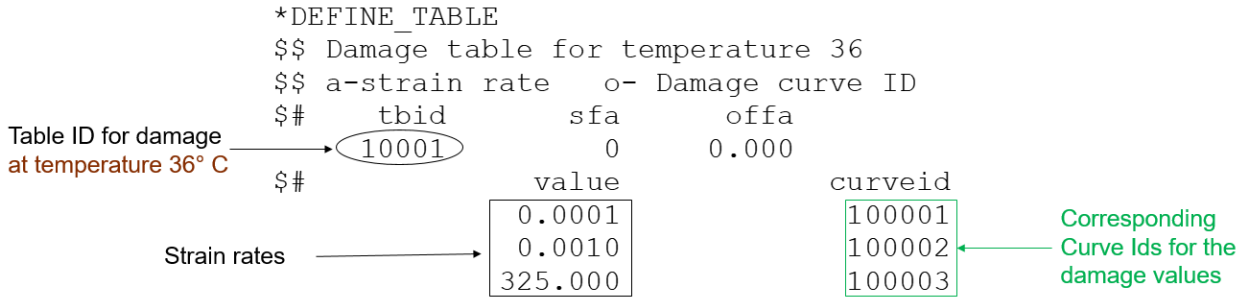

4. Each of the *DEFINE_CURVE curve IDs correspond to curves containing tabulated total strain-damage parameter data for each strain rates.

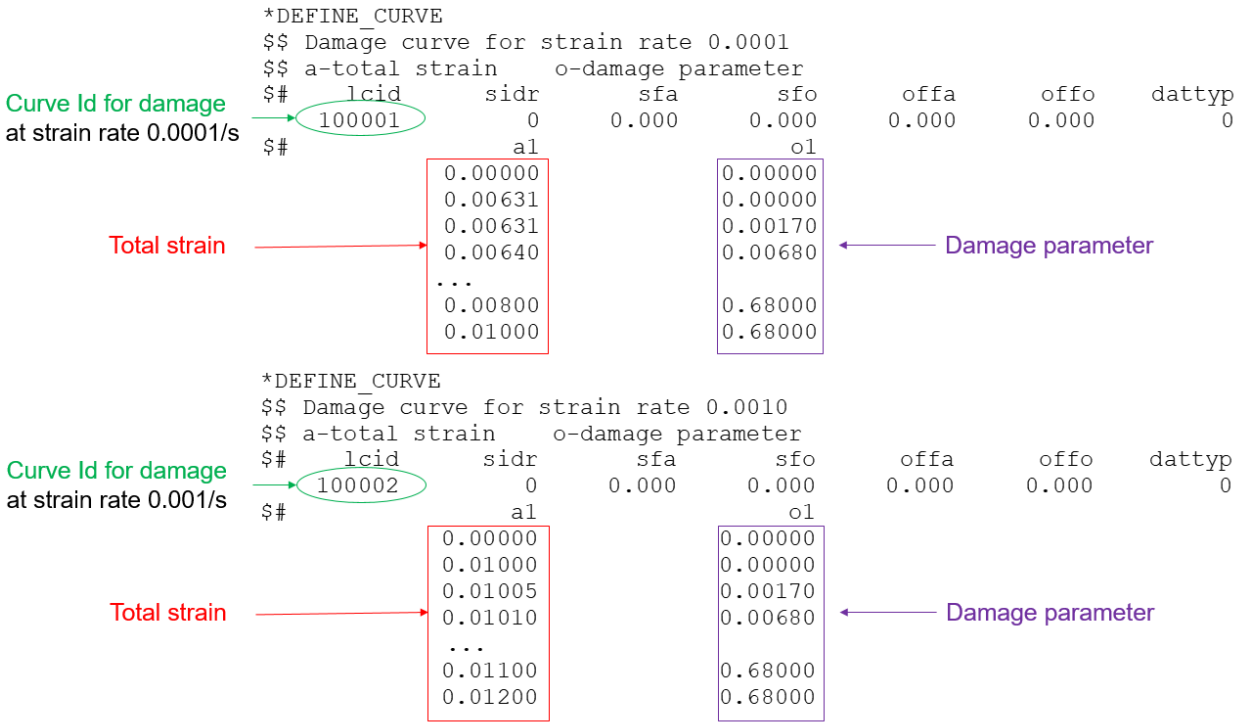

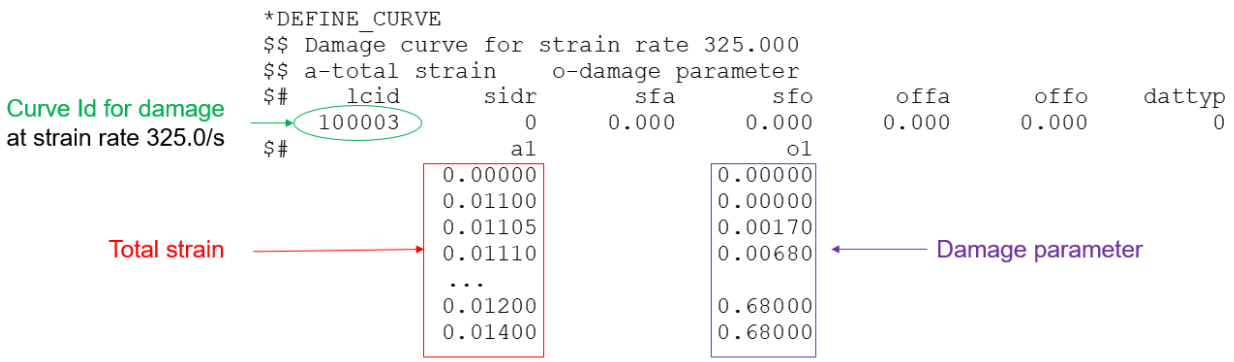

Note 6: Defining the damage parameters as d_{ij}^{kl} indicates damage being induced due to loading in direction ***ij*** and the reduction of stiffness has manifested in direction ***kl***. Uncoupled damage parameters have ***ij=kl*** while coupled damage parameters have ***ij≠kl***. The total strain values in the illustration above always correspond to the direction ***ij*** while the damage parameters correspond to direction ***kl***.

Note 7: Based on the input stress-total strain curve (Section 3.1.8), the following should be noted: *Uncoupled damage example*: If defining the uncoupled 2-direction compression damage parameter $\left(d_{22_C}^{22_C}\right)$ the total strain range (beginning and end values) in the damage parameter-total strain curve and the 2-direction compression stress-total strain curve should be the same.

Coupled damage example: If defining the coupled 2-direction compression 2-direction tension damage parameter $\left(d_{22_C}^{22_T}\right)$ the total strain range (beginning and end values) in the damage parameter-total strain curve and the 2-direction compression stress-total strain curve should be the same.

3.3 Failure Sub-Model

Three different failure models are implemented in MAT_213 and they can be activated one at a time. These are Puck Failure Criteria (PFC), Tsai-Wu Failure Criteria (TWFC) and Generalized Tabulated Failure Criteria (GTFC). Out of these three failure models, GTFC is driven by tabulated parameters. The number of parameters required are different for each of the implemented failure sub-model. The following sub-sections describe the input parameters required to drive each one of the failure models.

3.3.1 Input required for Puck Failure Criteria (PFC)

PFC is designed to be used only for unidirectional fiber reinforced composites. The failure onset of the material is predicted by the failure criterion, and a stress degradation model is used to degrade the material gradually [Shyamsunder et al., 2019; 2020c].

Table 3.6. Input parameters required to drive PFC

VARIABLE	DESCRIPTION
FV0	Γ_f : fiber direction fracture energy (a-direction) The current implementation does not distinguish between tension and compression fracture energies.
FV1	Post-peak residual damage in a-direction tension. Value must be a real number between 0 and 1. This value must be calibrated by the user.
FV2	Post-peak residual damage in a-direction compression. Value must be a real number between 0 and 1. This value must be calibrated by the user.
FV3	Post-peak residual damage in b/c-direction tension. Value must be a real number between 0 and 1. This value must be calibrated by the user.
FV4	Post-peak residual damage in b/c-direction compression. Value must be a real number between 0 and 1. This value must be calibrated by the user.
FV5	Post-peak residual damage in shear. Value must be a real number between 0 and 1. This value must be calibrated by the user.
FV6	m_{f} : magnification factor Recommended value for carbon fiber reinforced polymer (CFRP) composite is 1.1, and 1.3 for glass fiber reinforced polymer (GFRP) composite. [Deuschle and Kroplin, 2012]
FV7	p_{ba}^{t} : slope parameter: 0.30 (GFRP) and 0.35 (CFRP) [Deuschle and Kroplin, 2012]
FV8	p_{ba}^{c} : slope parameter: 0.25 (GFRP) and 0.30 (CFRP) [Deuschle and Kroplin, 2012]
FV9	p_{bb}^{t} : slope parameter: 0.20-0.25 (GFRP) and 0.25-0.30 (CFRP) [Deuschle and Kroplin, 2012]
FV10	p_{bb}^{c} : slope parameter: 0.20-0.25 (GFRP) and 0.25-0.30 (CFRP) [Deuschle and Kroplin, 2012]
FV11	ν_{ba}^{f} : fiber Poisson's ratio
FV12	E_{a}^{f} : fiber Young's modulus
FV13	Γ_1 : inter-fiber mode I fracture energy This value can be determined using double cantilever beam experiment. An example for obtaining the fracture energy of a unidirectional fiber reinforced composite is shown in Khaled et al. [2019a]
FV14	Γ_2 : inter-fiber mode II fracture energy This value can be determined using end-notched flexure experiment. An example for obtaining the fracture energy of a unidirectional fiber reinforced composite is shown in Khaled et al. [2019a]

3.3.2 Input required for Tsai-Wu Failure Criteria (TWFC)

TWFC can be used for any composite architecture [Hoffarth et al., 2020]. The element is degraded once the following criterion is satisfied $f^F(\sigma)$ reaches a value of 1.

$$f^F(\sigma) = \begin{pmatrix} F_1 & F_2 & F_3 & 0 & 0 & 0 \end{pmatrix} \begin{bmatrix} \sigma_{11} \\ \sigma_{22} \\ \sigma_{33} \\ \sigma_{12} \\ \sigma_{23} \\ \sigma_{31} \end{bmatrix} + \begin{bmatrix} \sigma_{11} \\ \sigma_{22} \\ \sigma_{33} \\ \sigma_{12} \\ \sigma_{23} \\ \sigma_{31} \end{bmatrix}^T \begin{bmatrix} F_{11} & F_{12} & F_{13} & 0 & 0 & 0 \\ F_{12} & F_{22} & F_{23} & 0 & 0 & 0 \\ F_{13} & F_{23} & F_{33} & 0 & 0 & 0 \\ 0 & 0 & 0 & F_{44} & 0 & 0 \\ 0 & 0 & 0 & 0 & F_{55} & 0 \\ 0 & 0 & 0 & 0 & 0 & F_{66} \end{bmatrix} \begin{bmatrix} \sigma_{11} \\ \sigma_{22} \\ \sigma_{33} \\ \sigma_{12} \\ \sigma_{23} \\ \sigma_{31} \end{bmatrix} \tag{3.20}$$

The yield function coefficients, F_{ij}, depend on the input failure stresses and are calculated as

$$\begin{aligned} F_1 &= \frac{1}{\widehat{\sigma}_{aa}^T} - \frac{1}{\widehat{\sigma}_{aa}^C} & F_{11} &= \frac{1}{\widehat{\sigma}_{aa}^T \widehat{\sigma}_{aa}^C} & F_{44} &= \frac{1}{\widehat{\sigma}_{ab}^2} \\ F_2 &= \frac{1}{\widehat{\sigma}_{bb}^T} - \frac{1}{\widehat{\sigma}_{bb}^C} & F_{22} &= \frac{1}{\widehat{\sigma}_{bb}^T \widehat{\sigma}_{bb}^C} & F_{55} &= \frac{1}{\widehat{\sigma}_{bc}^2} \\ F_3 &= \frac{1}{\widehat{\sigma}_{cc}^T} - \frac{1}{\widehat{\sigma}_{cc}^C} & F_{33} &= \frac{1}{\widehat{\sigma}_{cc}^T \widehat{\sigma}_{cc}^C} & F_{66} &= \frac{1}{\widehat{\sigma}_{ac}^2} \end{aligned} \tag{3.21}$$

$$F_{12} = -\frac{1}{2}\sqrt{F_{11}F_{22}} \tag{3.22}$$

$$F_{23} = -\frac{1}{2}\sqrt{F_{22}F_{33}} \tag{3.23}$$

$$F_{13} = -\frac{1}{2}\sqrt{F_{11}F_{33}} \tag{3.24}$$

Table 3.7. Input parameters required to drive TWFC

VARIABLE	DESCRIPTION
FV1	$\widehat{\sigma}_{aa}^{T}$: failure stress, tension, a-direction This can be taken as the peak stress/failure stress in the 1-direction tension curve in Fig. 3.1.
FV2	$\widehat{\sigma}_{aa}^{C}$: failure stress, compression, a-direction This can be taken as the peak stress/failure stress in the 1-direction compression curve in Fig. 3.1.
FV3	$\widehat{\sigma}_{bb}^{T}$: failure stress, tension, b-direction

	This can be taken as the peak stress/failure stress in the 2-direction tension curve in Fig. 3.1.
FV4	$\widehat{\sigma}_{bb}^{C}$: failure stress, compression, b-direction This can be taken as the peak stress/failure stress in the 2-direction compression curve in Fig. 3.1.
FV5	$\widehat{\sigma}_{cc}^{T}$: failure stress, tension, c-direction This can be taken as the peak stress/failure stress in the 3-direction tension curve in Fig. 3.1.
FV6	$\widehat{\sigma}_{cc}^{C}$: failure stress, compression, c-direction This can be taken as the peak stress/failure stress in the 3-direction compression curve in Fig. 3.1.
FV7	$\widehat{\sigma}_{ab}$: failure stress, shear, a-b plane This can be taken as the peak stress/failure stress in the 1-2 plane shear curve in Fig. 3.1.
FV8	$\widehat{\sigma}_{bc}$: failure stress, shear, b-c plane This can be taken as the peak stress/failure stress in the 2-3 plane shear curve in Fig. 3.1.
FV9	$\widehat{\sigma}_{ac}$: failure stress, shear, a-c plane This can be taken as the peak stress/failure stress in the 1-3 plane shear curve in Fig. 3.1.

3.3.3 Input required for Generalized Tabulated Failure Criteria (GTFC)

GTFC can be used for any composite architecture [Shyamsunder et al., 2020a, 2020c] and has a strain-based criterion for element erosion. The following set of equations are used to compute the GTFC parameters – equivalent failure strains (ε_{IP}^{eq}, ε_{OOP}^{eq}) and failure angles (θ_{IP}, θ_{OOP}),

$$\varepsilon_{IP}^{eq} = \sqrt{\varepsilon_{11}^2 + \varepsilon_{22}^2 + 2\varepsilon_{12}^2} \tag{3.25}$$

$$\theta_{IP} = \cos^{-1}\left(\frac{\sigma_{22}}{\sqrt{\sigma_{22}^2 + \sigma_{12}^2}}\right) \tag{3.26}$$

$$d_1 = \frac{\varepsilon_{IP}^{eq}}{\varepsilon_{IP}^{fail}} \tag{3.27}$$

$$\varepsilon_{OOP}^{eq} = \sqrt{\varepsilon_{33}^2 + 2\varepsilon_{13}^2 + 2\varepsilon_{23}^2} \tag{3.28}$$

$$\theta_{OOP} = \cos^{-1}\left(\frac{\sigma_{13}}{\sqrt{\sigma_{13}^2 + \sigma_{23}^2}}\right) \tag{3.29}$$

$$d_2 = \frac{\varepsilon_{OOP}^{eq}}{\varepsilon_{OOP}^{fail}} \tag{3.30}$$

Table 3.8. Input parameters required to drive GTFC

VARIABLE	**DESCRIPTION**	
	SOLID	**SHELL**
FV1	n : In-plane and out-of-plane interaction term used in computing d if n = 0, d = max(d_1, d_2) else, $d = (d_1^n + d_2^n)^{\frac{1}{n}}$. This is a parameter which can be used for calibration purpose. It is recommended to start with a value of zero, which decouples the two modes of failure. An element is eroded if d reaches a value of 1	n/a
FV2	FCIP: Table ID for the table containing in-plane: $(\theta, \varepsilon_{fail})$ values with respect to specified a-direction stress.	FCIP: Table ID for the table containing: $(\theta, \varepsilon_{fail})$ values with respect to specified a-direction stress. An element is eroded if d_1 reaches a value of 1 [Achstetter, 2019]. It should be noted that *DEFINE_ELEMENT_EROSION_SHELL keyword is required for element erosion.
FV3	FCOOP: Table ID for the table containing out-of-plane: theta (θ) – radius (r) values with respect to specified normal c-direction stress. NOT required for shell element	

Like the deformation sub-model, the entirety of the GTFC parameter data must be organized into a set of curves.

i. Define FCIP and FCOOP in the MAT_213 input deck. These are DEFINE_TABLE IDs for in-plane and out-of-plane failure surface, respectively.

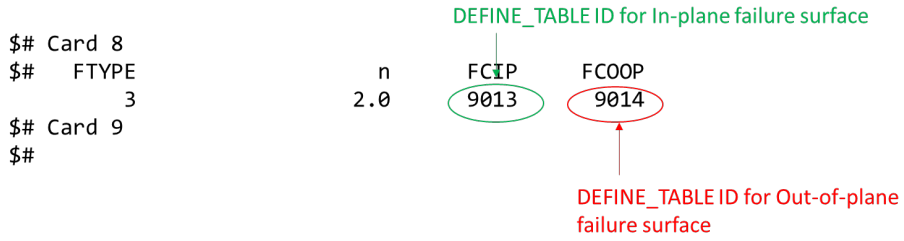

ii. The FCIP DEFINE_TABLE ID contains the 1-direction stresses for which the in-plane failure surface is available. The theta-radius curve IDs corresponding to each 1-direction stress are not included in the *DEFINE_TABLE definition (see below).

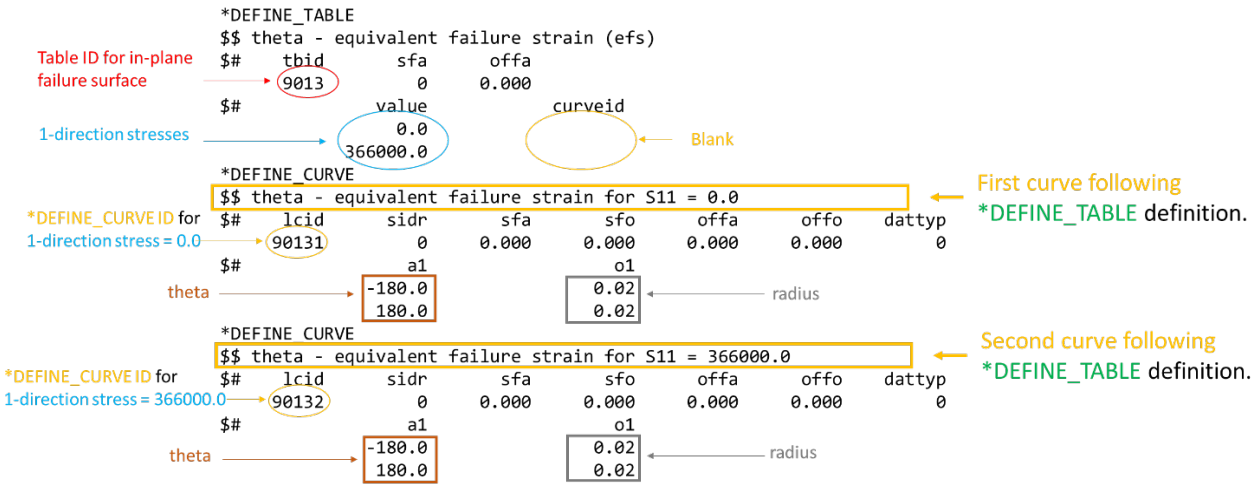

iii. Immediately following the end of the definition of the *DEFINE_TABLE definition, the curves corresponding to each 1-direction stress are defined in the same order as what is provided in the *DEFINE_TABLE definition.

iv. Each of the *DEFINE_CURVE curve IDs correspond to curves containing tabulated theta-radius data for each of the 1-direction stress.

v. In a similar manner, the out-of-plane failure surface in the form of theta-radius can be defined.

4. MAT_213 Error and Warning Messages

The following table shows the error (E) and the warning (W) messages from MAT_213. These messages are visible on the terminal or command prompt as well as in the DYNA message file. These messages are divided into two parts – the first part shown in Table 4.1 are detected and handled inside the MAT_213 subroutines while the second part shown in Table 4.2 are detected and handled within DYNA's input data checks. A sum of alphabets and numbers is used to format the string for error and warning numbers based on where they are detected as follows:

a) Format of errors and warnings detected in pre-processing (PP) is INI +<#>.
b) Format of errors and warning detected during simulation (S) is SOL+<#>.
c) Format of errors and warnings detected by DYNA's input data checks is KEY+<#>.

Table 4.1. Error and Warning Messages

E/W #	E/W	Message or Warning	Where Detected	Fix
INI+440	E	MAT_213 table and curve input: Curve # <#> in Table (<#>) of Table_3D (<#>) is not a curve.	PP	*DEFINE_CURVE should be used to input a curve.
INI+441	E	MAT_213 table and curve input: Table # <#> in Table 3D (<#>) does not refer to a table.	PP	For a given *DEFINE_TABLE_3D definition, TABLE ID should be entered corresponding to the given temperature values(s).
INI+442	E	MAT_213 table and curve input: Table # <#> in table 3D (TABLE_3D ID #) does not refer to a table.	PP	For a given *DEFINE_TABLE_3D definition, TABLE ID should be entered corresponding to the given temperature values(s).
INI+443	E	MAT_213 table and curve input: Input ID (<ERRONEOUS ID #>) in material card does not refer to a table 3D ID.	PP	LT1 through LT12 should be TABLE_3D ID's.
INI+444	E	MAT_213 table and curve input: Curve ID <ERRONEOUS ID #> which refers to the yield strain curve in the material card <#> is not a curve ID.	PP	YSC value must be a curve ID

INI+445	E	MAT_213 table and curve input: Curve ID <curve ID> is missing in initial yield stress data curve.	PP	Yield strain values should be specified for all the stress-strain curves in the input deck.
INI+446	E	MAT_213 conversion stress/strain curve input: itest <#> does not have a value between 1 and 12.	PP	This is an internal check within LS-DYNA.
INI+468	E	MAT_213 table and curve input: Negative strain data detected for normal or shear direction input curve id <#>.	PP	There should be no negative value in the strain data.
INI+469	E	MAT_213 table and curve input: Strain values not in ascending order. Please check curves corresponding to TABLE_3D <TABLE_3D ID#>	PP	Strain values should be in ascending order.
INI+470	E	MAT_213 table and curve input: Effective stress values are not in ascending order after curve conversion: curve id <#>.	PP	The stresses in the input deck should be such that the effective stress values computed after the pre-processing step should be in ascending order.
INI+492	E	MAT_213 table and curve input: Curve ID <#> which refers to a damage curve ID in the material card <#> is not a curve ID.	PP	DC value must be a curve ID
INI+493	E	Input strain rate for curve ID <curve ID> should be greater than or equal to 0.0	PP	The strain rate value specified for any stress-strain input curve cannot be negative.
INI+494	E	Damage parameter IDs in curve# <damage curve ID> must be between 1 and 84	PP	In the *DEFINE_CURVE for damage curve, the abscissa values which are the damage parameters, should be a number between 1 through 84.
INI+495	E	Yield strain value for curve# <curve id#> should be greater than 0.0.	PP	Yield strain value should be greater than 0.0.

INI+496	W	Yield strain value corresponding to curve <curve ID> should be greater than the ultimate strain for linear elastic behavior.	PP	For a given curve, if the corresponding flow rule coefficient value is zero, the yield strain value specified should be greater than the ultimate strain for the curve.
INI+514	E	MAT_213: FV0 (Ga) set to <#> but cannot be less than or equal to zero.	PP	This error occurs when the fracture energy in the fiber direction is set less than or equal to zero corresponding to FTYPE = 1.
INI+515	E	MAT_213: PPRD set to <#> but cannot be less than zero.	PP	This error occurs when at least one of the post-peak residual damage values input are less than zero corresponding to FTYPE = 1.
INI+516	E	MAT_213: Input parameter is set to <#> but cannot be less than zero.	PP	This error occurs if anyone of the parameters – FV6, FV7, FV8, FV9, FV10, FV11, FV12, FV13 or FV14, is less than or equal to zero.
INI+517	E	MAT_213: Input strength is set to <#> but cannot be less than or equal to zero.	PP	This error occurs if any of the strength values corresponding to FTYPE=2 is zero. The strength values should be positive.
INI+518	E	MAT_213: FV2 has to be a TABLE_ID.	PP	This error occurs when FV2 is not a *DEFINE_TABLE ID. This corresponds to FTYPE = 3 using SHELL element.
INI+519	E	MAT_213: FV1 is set to <#> but cannot be less than zero.	PP	This error occurs when FV1 is less than zero, corresponding to FTYPE = 3 using SOLID element.

INI+520	E	MAT_213: FV2 is set to <#> and FV3 is set to <#> but they have to be table IDs.	PP	This error occurs when either or both FV2 and FV3 are not *DEFINE_TABLE ID(s). This corresponds to FTYPE = 3 using SOLID element.
INI+521	E	MAT_213: DCFLAG is set to <#> but has to be either 0 or 1.	PP	
INI+522	E	MAT_213: CP is set to <#> but cannot be negative.	PP	
INI+523	E	MAT_213: TQC is set to <#> but cannot be negative.	PP	
INI+566	E	MAT_213: Inconsistency in the stress-strain curves or flow rule coefficients. Please ensure that the flow rule coefficient values for the elastic components are zero.	PP	In the pre-processing step, during the conversion of strains into effective plastic strain, the effective plastic strain is equally spaced using an increment. This error will be detected if this increment is less than or equal to zero. This will also happen if there is inconsistency in material input data. The user must make sure that all the input parameters - flow rule coefficients, yield strains, stress-strain curves, damage parameters, etc. are physical.
INI+567	E	MAT_213: negative stress data detected for normal or shear direction input curve (<#>)	PP	There should not be any negative stress value for the normal and the shear component of the stress-strain input curves.
INI+568	E	MAT_213: Inconsistency in the yield strain values specified in YSC (curve ID <#>). Either the	PP	Yield strain values should be greater than zero. Also check whether the yield strain values are

		yield strain values are entered as zeros or the values are missing.		specified for all the stress-strain curves in the input deck.
INI+569	W	MAT_213: Inconsistency in the yield strain values specified in YSC. Either the yield strain values are entered as zeros or the values are missing.	PP	Yield strain values should be greater than zero. Check whether the yield strain values are specified for all the stress-strain curves in the input deck.
INI+570	E	MAT_213: Negative plastic strain computed during curve conversion. Curve: <#>	PP	This error is detected during the process of converting strain into plastic strain and arises if any computed plastic strain values is/are negative. Apart from checking the input data for consistency, the user can also try to reduce the value of the yield strain.
INI+571	E	Strain-damage parameter data set cannot be defined using a combination of DEFINE_CURVE and DEFINE_TABLE_3D	PP	This error is detected when damage parameter is defined using a combination of DEFINE_CURVE and DEFINE_TABLE_3D. Use either DEFINE_CURVE or DEFINE_TABLE_3D.
INI+572	E	Damage curve not defined corresponding to strain-rate	PP	This error is detected when the stress strain curve is defined for different strain rates and damage curve is missing for at least one-strain rates.
INI+573	E	Damage curve not defined corresponding to temperature	PP	This error is detected when the stress strain curve is defined for different temperatures and damage curve is

				missing for at least one temperature.
SOL+1357	E	MAT_213: Convexity Conditions for Flow Rule Not Met - element id <#>.	S	Choose Flow Rule coefficients to satisfy convexity conditions.
SOL+1358	E	MAT_213: Convexity Conditions for Yield Function Not Met After Correction (Fcheck1) - element id <#>.	S	$F_{11}F_{22} - F_{12}^2 < 0$ The input stress-strain curves in the 1 and 2-direction need to be modified to have a convex yield surface at any given effective plastic strain value.
SOL+1359	E	MAT_213: Convexity Conditions for Yield Function Not Met After Correction (Fcheck2) - element id <#>.	S	$F_{33}F_{22} - F_{23}^2 < 0$ The input stress-strain curves in the 2 and 3-direction need to be modified to have a convex yield surface at any given effective plastic strain value.
SOL+1360	E	MAT_213: Convexity Conditions for Yield Function Not Met After Correction (Fcheck3) - element id <#>.	S	$F_{11}F_{33} - F_{13}^2 < 0$ The input stress-strain curves in the 1 and 3-direction need to be modified to have a convex yield surface at any given effective plastic strain value.
SOL+1361	E	MAT_213: Inconsistency in the stress-strain curves or flow rule coefficients. Please ensure that the flow rule coefficient values for the elastic components are zero - element id <#>.	S	This error is detected during the simulation, when the initial estimate of plastic multiplier increment which is set as the upper bound for the secant iteration is Not a Number (NaN).
SOL+1362	E	MAT_213: Could not bound plastic multiplier increment - element id <#>.	S	This condition arises when the plastic multiplier increment upper bound cannot be obtained. One fix is to reduce the TSSFAC value.

SOL+1364	E	MAT_213: Inconsistency in the stress-strain curves or flow rule coefficients. Please ensure that the flow rule coefficient values for the elastic components are zero - element id <#>	S	This error is detected when the estimate of plastic multiplier increment is NaN during secant iteration. This will happen if there is inconsistency in material input data. The user must make sure that all the input parameters - flow rule coefficients, yield strains, stress-strain curves, damage parameters, etc. are physical.
SOL+1365	E	MAT_213: Estimate of plastic multiplier increment is negative during secant iteration - element id <#>.	S	This error arises if there is inconsistency in material input data. The user must make sure that all the input parameters - flow rule coefficients, yield strains, stress-strain curves, damage parameters, etc. are physical. This can also be due to numerical instability in the finite element simulation.
SOL+1366	E	MAT_213: Yield function tolerance (PTOL) not met - element id <#>.	S	If for a given plastic multiplier increment value the yield function value is less than PTOL, then the current plastic multiplier is used for the radial return. This error can be avoided if the value of PTOL is increased. Note that the accuracy of the prediction/response may be reduced.
SOL+1368	E	MAT_213: Curve id missing in initial yield strain values (YSC) - element id <#>.	S	Yield strain values should be specified for all the

				stress-strain curves in the input deck.
SOL+1371	E	MAT_213: Convexity Conditions for Yield Function Not Met After Correction (Fcheck1).yf - element id <#>.	S	The input stress-strain curves in the 1 and 2-direction need to be modified to have a convex yield surface at any given effective plastic strain value.
SOL+1372	E	MAT_213: Convexity Conditions for Yield Function Not Met After Correction (Fcheck2).yf - element id <#>.	S	The input stress-strain curves in the 2 and 3-direction need to be modified to have a convex yield surface at any given effective plastic strain value.
SOL+1373	E	MAT_213: Convexity Conditions for Yield Function Not Met After Correction (Fcheck3).yf - element id <#>.	S	The input stress-strain curves in the 1 and 3-direction need to be modified to have a convex yield surface at any given effective plastic strain value.
SOL+1398	E	MAT_213: Secant solver: Cannot bound plastic multiplier increment - element id <#>.	S	One fix is to reduce the TSSFAC value.
SOL+1410	E	MAT_213 cannot be used with 3D thick shell formulation.	S	
SOL+1440	E	PR21, PR31, PR32 not thermodynamically admissible - element id <#>.	S	This error is detected when MAT_213 internal algorithm cannot fix the Poisson's ratios to be compatible with material orthotropy. Decrease Poisson's ratio values which are large in magnitude.
SOL+1446	E	MAT_213: conversion stress/strain curve input: itest (1) value should be between 1 and 12 - element id <#>.	S	This is an internal check within LS-DYNA.
SOL+ 1496	W	Convexity corrections made for yield surface	S	The input stress-strain curves need to be

				modified to have a convex yield surface at any given effective plastic strain value.
SOL + 1497	W	Element erosion - negative volume in element #:<#>	S	If volume of any element is detected as negative.
SOL + 1498	W	Element erosion - strain criterion (e11 > ef11) in element #: <#>	S	
SOL+ 1499	W	Element erosion - 1 direction stress reversal in element #:<#>	S	
SOL + 1500	W	Element degraded IFF in element #:<#>	S	If inter fiber fracture is detected in the puck failure criterion, then stresses components other than 1 direction are degraded.
SOL +1501	W	Element erosion - damage criterion in element #: <#>	S	If the effective damage parameter is greater than 1 in the puck failure criterion.
SOL+ 1502	W	Element erosion - 2 direction stress reversal in element #:<#>	S	
SOL + 1503	W	Element erosion - 3 direction stress reversal in element #:<#>	S	
SOL + 1504	W	Element erosion - 12 shear stress reversal in element #:<#>	S	
SOL+ 1505	W	Element erosion - 23 shear stress reversal in element #:<#>	S	
SOL + 1506	W	Element erosion - 13 shear stress reversal in element #:<#>	S	
SOL + 1507	W	Element erosion – failure parameter > 1.0 (GTFC) in element <#>	S	If failure parameter d is greater than 1 in the general tabulated failure criterion.

Table 4.2 Error and Warning Messages

E/W #	E/W	Message or Warning
KEY+1208	W	Invalid PTOL value in line <#>. PTOL should be greater than 0.0. PTOL has been set to 1.0E-06.
KEY+1209	E	Invalid TCSYM value in line <#>. The value should be between 0 and 5.
KEY+1210	E	Invalid FTYPE value in line <#>. FCTYPE should be 0, 1, 2 or 3.

KEY+1312	E	VEVP = <#> VEVP should be 0, 1 or 2.
KEY+1313	E	PMACC = <#> PMACC has to be a positive integer greater than 1. It is set to a default value of 1000 if left blank or input as 0.
KEY+1314	E	Decay constant should not be negative BETA = <#>

5. Frequently Asked Questions

The following are some of the questions raised by MAT_213 users.

1. What does MAT_213 do if information is needed beyond the end of any stress-strain curve?
   Answer: If data is needed beyond the end of the user input curve, an extrapolation is performed using the last two points on the curve.

2. In the Fig. 5.1(a), *Model Curve* is the input stress-strain curve for 1-direction tension component using the primary axis and *Damage Curve* which is the input damage curve in the uncoupled 1-direction tension using the secondary axis. Fig. 5.1(b) shows the corresponding input for 1-direction compression component with zero damage. How to model a material with the following input stress-strain and damage curve? What value of H_{11} should be used? What value of yield strain should be used? Do the input curves need to be modified for numerical stability?

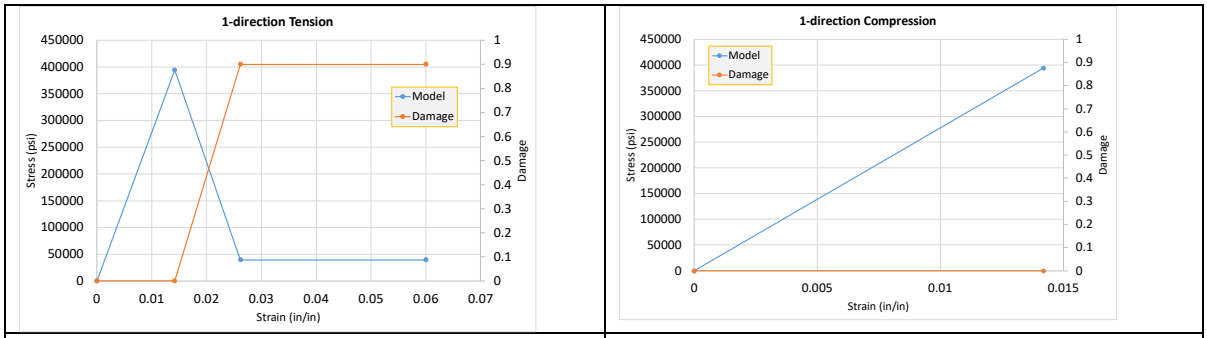

(a) (b)

Fig. 5.1. Input *Model Curve* and damage curve for (a) 1-direction tension and (b) 1-direction compression

Answer: Section 3.2.3 provides general information on this type of input. Fig. 5.1 shows plasticity behavior needs to be activated in 1-direction tension but, on the other hand the stress-strain relationship is linearly elastic. Hence a very small value needs to be specified for H_{11} (= 0.01). The yield strain values need to be $\varepsilon_y^T = 0.0142$ and $\varepsilon_y^C = 0.0142$, corresponding to the peak stress values. Since, H_{11} is non-zero, MAT_213 assumes that there is plasticity in the 1-direction and hence, the plastic strains are computed in the pre-processing step. In this example, the plastic strains computed for each data point will turn

out to be negative since the compression curve is entirely linear. MAT_213 will generate an error message. To avoid the error message, a numerically small plasticity needs to be introduced by modifying the compression curve by having an additional strain data point $(\varepsilon = 0.0145)$ added at the end of the curve as shown in Fig. 5.2.

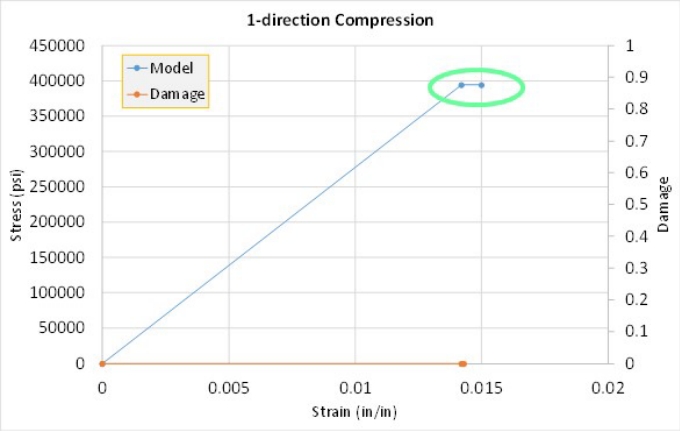

Fig. 5.2. Modified 1-direction compression input

3. What does the following warning message mean?
   "Yield strain value corresponding to curve <#> should be greater than the ultimate strain for linear elastic behavior"

   If the yield strain is beyond the end of the linear part of the stress-strain curve, a modulus will be computed that is smaller than the initial slope of the curve leading to a negative plastic strain when there is curve conversion in the pre-processing step.

   Answer: This warning is for **elastic component only** (flow rule coefficient = 0) is generated by the program if the yield strain is less than the ultimate strain; otherwise, a negative plastic strain value will be generated. For example, for the T800-F3900 composite, since the 1-direction component is assumed to be fully elastic, a yield strain value which is greater than the ultimate strain in 1-direction is used in the input. The ultimate strain in 1-direction tension and compression are 0.0156 and 0.006, respectively. Fig. 5.3 shows the yield strain values corresponding the curve id's. Curve id's 1 and 4 correspond to 1-direction tension and compression, respectively. Since a value greater than the ultimate strains (0.0156 and 0.006, respectively) are needed, a value "1.00" for both 1-direction tension and compression is used.

   This check (checking whether the yield strain value is greater than the ultimate strain) is **not done** if the flow rule coefficient value (H) is non-zero (there is plasticity in the input stress-strain curve corresponding to this non-zero H). For this scenario, the yield strain value is the strain value corresponding to the end of the elastic regime in the curve. For example, in Fig. 5.3, the curve id 2 corresponds to 2-direction tension that has plasticity. The ultimate strain for this curve is 0.006.

The warning message is generated most likely because the input has a flow rule coefficient value of 0 corresponding to curve <#>.

```
*KEYWORD
*DEFINE_CURVE
$$ Curve of initial yield strain values
$$ a-Curve ID's     o-Initial Yield Strain
$#     lcid      sidr       sfa       sfo
       100         0     0.000     0.000
$#                a1                   o1
$Strain Rate:1; Temp:21
                   1                1.00000
                   2                0.00267
                   3                0.00160
                   4                1.00000
                   5                0.00830
                   6                0.00688
                   7                0.00300
                   8                0.00025
                   9                0.00810
                  10                0.00160
                  11                0.00860
                  12                0.00496
$ Strain Rate:1; Temp:50
```

Fig. 5.3. Yield strain values for T800/F3900 composite

4. "Twelve physical or numerical experiments must be performed under quasi-static and room temperature (QS-RT) conditions to characterize a solid element model". Is this strictly required? What if one is interested in simulations using high rate data only. Would one be forced to generate QS-RT data in order to generate a working model?

   Answer: There is no need for QS-RT data if the user is only interested in the high rate data simulations. Please refer to Remark 2 of the keyword manual for general information.

5. Is it possible to simplify the input deck assuming material symmetry?

   Answer: Yes. For example, in case of a transversely isotropic material, the material properties entered for the 2 and the 3-direction can be made equal.

References (Arranged by last name of first author/entity)

T. Achstetter (2019). “Development of a composite material shell-element model for impact applications”, *PhD Dissertation,* George Mason University.

H.M. Deuschle, and B.H. Kroplin (2012). “Finite element implementation of Puck's failure theory for fiber-reinforced composites under three-dimensional stress”, *J Composite Materials*, 46(19-20), 2485-2513, 2012.

C. Hoffarth, S.D. Rajan, R. Goldberg, K. Carney, P. DuBois, and G. Blankenhorn (2016). “Implementation and Validation of a Three-Dimensional Plasticity-Based Deformation Model for Orthotropic Composites”, *Composites A*, http://dx.doi.org/10.1016/j.compositesa.2016.10.024, 91:1, 336-350, December 2016.

C. Hoffarth, B. Khaled, L. Shyamsunder, S.D. Rajan, R. Goldberg, K. Carney, P. DuBois, and G. Blankenhorn (2017). “Verification and Validation of a Three-Dimensional Orthotropic Plasticity Constitutive Model Using a Unidirectional Composite”, *Fibers*, 5(1), 12; doi:10.3390/fib5010012, March 2017.

C. Hoffarth, B. Khaled, L. Shyamsunder, and S.D. Rajan (2020). “Development of a Tabulated Material Model for Composite Material Failure, MAT213: Theory, Implementation, Verification & Validation”, Technical Report, DOT/FAA/TC-19/50, Federal Aviation Administration, January 2020.

R. Goldberg, K. Carney, P. DuBois, C. Hoffarth, J. Harrington, S.D. Rajan and G. Blankenhorn (2016). “Development of an Orthotropic Elasto-Plastic Generalized Composite Material Model Suitable for Impact Problems”, *ASCE J of Aerospace Engineering*, doi: 10.1061/(ASCE)AS.1943-5525.0000580. Dec 2015. Also 29:4, 1-11, 2016.

R. Goldberg, K. Carney, P. DuBois, C. Hoffarth, B. Khaled, S.D. Rajan and G. Blankenhorn (2018a). “Analysis and Characterization of Damage Utilizing a Generalized Composite Material Model Suitable for Impact Problems”, *ASCE J of Aerospace Engineering*, 10.1061/(ASCE)AS.1943-5525.0000854, March 2018.

R. Goldberg, K. Carney, P. DuBois, C. Hoffarth, B. Khaled, L. Shyamsunder, S.D. Rajan and G. Blankenhorn (2018b). “Implementation of a Tabulated Failure Model into a Generalized Composite Material Model”, *J of Composite Materials*, https://doi.org/10.1177/0021998318786778, July 10, 2018.

J. Harrington, C. Hoffarth, S.D. Rajan, R. Goldberg, K. Carney, P. DuBois, and G. Blankenhorn (2017). “Using Virtual Tests to Complete the Description of a Three-Dimensional Orthotropic Material”, *ASCE J of Aerospace Engineering*, DOI: 10.1061/(ASCE)AS.1943-5525.0000737, March 2017.

A.S. Kaddour, M.J. Hinton, S. Li, P.A. Smith (2014). The World-Wide Failure Exercises: How Can Composites Design and Manufacture Communities Build Their Strength. In Proceedings of the *16th European Conference on Composite Materials* (ECCM16), Seville, Spain, 22–26 June 2014.

B. Khaled, L. Shyamsunder, C. Hoffarth, S.D. Rajan, R.K. Goldberg, K.S. Carney, P. DuBois, and G. Blankenhorn (2017a). "Experimental Characterization of Composites to Support an Orthotropic Plasticity Material Model", *J of Composite Materials*, DOI: 10.1177/0021998317733319, August 2017.

B. Khaled, L. Shyamsunder, C. Hoffarth, S.D. Rajan, R.K. Goldberg, K.S. Carney, P. DuBois, and G. Blankenhorn (2017b). "Damage Characterization of Composites to Support an Orthotropic Plasticity Material Model", *J of Composite Materials*, doi:10.1177/0021998318793506, August 2018.

B. Khaled, L. Shyamsunder, N. Holt, C. Hoover, S.D. Rajan, and G. Blankenhorn (2019a). "Enhancing the Predictive Capabilities of a Composite Plasticity Model Using Cohesive Zone Modeling", *Composites A*, doi:10.1016/j.compositesa.2019.03.001, March 2019.

B. Khaled (2019b). "Experimental Characterization and Finite Element Modeling of Composites to Support a Generalized Orthotropic Elasto-Plastic Damage Material Model for Impact Analysis", *PhD Dissertation*, Arizona State University, Tempe, US. **Also available as FAA Technical Report: DOT/FAA/TCTT-22/39, Nov 2022.**

NASA (2016). Available online: https://www.nasa.gov/press/2015/april/nasa-creates-partnership-to-advance-composite-materials-for-aircraft-of-the-future (accessed 28 November 2016).

S. Ogihara and K.L. Reifsnider (2002). "Characterization of Nonlinear Behavior in Woven Composite Laminates", *Applied Composite Materials*, 9, 249-263.

L. Shyamsunder, B. Khaled, S.D. Rajan, R.K. Goldberg, K.S. Carney, P. DuBois, and G. Blankenhorn (2019). "Implementing Deformation, Damage and Failure in an Orthotropic Plastic Material Model", *J of Composite Materials*, DOI: 10.1177/0021998319865006, July 2019.

L. Shyamsunder (2020a). "Failure Modeling in an Orthotropic Plastic Material Model for Impact and Crush Analysis", PhD Dissertation, School of Sustainability and Built Environment, Arizona State University, Tempe. Also available as **FAA Technical Report: DOT/FAA/TCTT-22/38, Nov 2022.**

L. Shyamsunder, B. Khaled, S.D. Rajan, and G. Blankenhorn (2020b). "Failure Modeling in an Orthotropic Plasticity Material Model", accepted to the *ASCE Earth and Space Conference*, April 2020.

L. Shyamsunder, B. Khaled, and S.D. Rajan (2020c). “MAT 213 V1.3.5 Status”, *FAA Teleconference* March 25, 2020, Aerospace Working Group.

L. Shyamsunder, B. Khaled, S.D. Rajan, M. Pereira, P. DuBois, and G. Blankenhorn (2022a). “Numerical Validation of Composite Panel Impact Tests”, *J of Impact Engineering*, https://doi.org/10.1016/j.ijimpeng.2021.104032, September 2021; 159:1-15, January 2022.

L. Shyamsunder, A. Maurya, S.D. Rajan, D. Cordasco. D. Revilock, and G. Blankenhorn, “Impact Simulation of Composite Panels for Aerospace Applications”, *Composites B*, https://doi.org/10.1016/j.compositesb.2022.110320, September 2022.

C.T. Sun and J.L. Chen (1989). “A Simple Flow Rule for Characterizing Nonlinear Behavior of Fiber Composites”, *Journal of Composite Materials*, 23:10, 1009-1020.

Toray Carbon Fibers America (2020). https://www.toraycma.com/ (last accessed June 28, 2020).